eman ta zabal zazu
Universidad del País Vasco
Euskal Herriko Unibertsitatea
ZIENTZIA ETA TEKNOLOGIA FAKULTATEA
FACULTAD DE CIENCIA Y TECNOLOGÍA

Bachelor Thesis
Physics Degree

An analysis of the topological properties of the electronic band structure using simple tight-binding models

Author:
Mireia Tena Zuazolacigorraga
Director:
Luis Ángel Elcoro Cengotitabengoa

July 2021, Leioa

Contents

Chapter 1

Introduction

One of the early successes of quantum mechanics was the creation of *Band Theory* and its ability to predict the vastly different electrical conductivities of different materials. No classical theory could explain the origin of the unalike conductivities, that could vary in more than twenty orders of magnitude.

The first version of Band Theory was developed in the 1930s, and its pinnacle was the classification of crystals into insulators and metals depending on whether the band structure contained or not a partially filled band. This theory relied on two main pillars: Bloch's theorem, which rules the behavior of an electron in the periodic potential created by ions, and Fermi–Dirac statistics, which governs the filling of energy bands by electrons.

In the 1980s, the experimental discovery of the integer Quantum Hall Effect and its subsequent theoretical understanding as a Berry phase effect, provided a completely new perspective. In 1988, Haldane clearly spelled out that the Anomalous Quantum Hall Effect (AQHE), where there is no external uniform magnetic field nor Landau levels, was also a particular instance of a Berry phase effect, provided time reversal symmetry was broken. The field of topological phases of matter has been developed ever since, and is of great interest in present times.

The aim of this work is to present the basic concepts of topological band theory, restricted to two-dimensional insulators that can be characterized by the Chern number (AQHE systems), and to theoretically and computationally study the model for a honeycomb lattice proposed by Haldane. For that purpose, the tight binding approximation will be used, with the help of second quantization formalism.

A theoretical background with the necessary knowledge to follow this work is given in Chapter 2, which is divided in three parts. The first one contains a review of some basic aspects of band theory. The second section is focused on the use of the second quantization formalism in tight-binding models. Finally, the last section of this chapter explains the role of topology in the particular case of interest.

In Chapter 3, the theory is applied to the study of Haldane's model. Important phenomena will be deduced directly from the first principles presented in the previous chapter. The tight-binding models will be analytically and computationally solved, and the computational tools used will be explained.

In the last chapter, Chapter 4, the principal conclusions of the previous sections will be underlined, with the addition of some final comments about the studied subject.

Chapter 2

Theoretical background

2.1 Electrons in a crystal

The aim of this section is to briefly explain some basic concepts and results regarding band theory. I will start with the description of a metallic solid as a perfectly periodic structure, and arrive to the solution of the Schrödinger equation in the independent electron approximation.

2.1.1 Crystal structure

Any crystalline solid can be modeled as a perfectly periodic arrangement of atoms, that are sitting still on their corresponding sites. This periodicity implies a spacial translational symmetry. We will now review some of the most important geometrical properties of these periodic structures.

Bravais lattice. The underlying lattice of the crystal structure that holds the translational symmetry is called a *Bravais lattice*. A m-dimensional Bravais lattice consists of all points given by position vectors $\mathbf{R}$ of the form:

$$\boldsymbol{R} = \sum_{i=1}^{m} n_i \boldsymbol{e}_i \tag{2.1}$$

where n_i are integers and vectors $\boldsymbol{e}_i$ don't lie in the same m-1 dimensional surface. Vectors $\mathbf{R}$ connect the repeated units of the crystal.

Primitive vectors. The vectors $\boldsymbol{e}_i$ that generate the lattice are called the *primitive vectors* of the lattice.

Primitive unit cell. A *primitive unit cell* is a volume that when translated through all vectors $\mathbf{R}$ just fills all space, without voids and without overlapping.

The basis. We need a *basis* to describe the arrangement of the ions within a primitive unit cell. This basis is the physical unit that repeats itself at all points in the Bravais lattice.

Lattice with a basis. To sum up, the crystal structure is described by giving the underlying Bravais lattice, and the basis with the locations of the ions that is attached to each point in the Bravais lattice.

2.1.2 The reciprocal lattice

The *reciprocal lattice* is defined as the set of all wave vectors $\boldsymbol{K}$ that give plane waves with the same periodicity as the Bravais lattice. Being $\boldsymbol{R}$ a vector of the direct lattice, vectors $\boldsymbol{K}$ must satisfy:

$$e^{i\boldsymbol{K}\cdot(\boldsymbol{r}+\boldsymbol{R})} = e^{i\boldsymbol{K}\cdot\boldsymbol{r}} \quad \longrightarrow \quad e^{i\boldsymbol{K}\cdot\boldsymbol{R}} = 1 \tag{2.2}$$

If $\boldsymbol{b}_i$ are the primitive vectors of the reciprocal lattice, it follows from condition (2.2) that these relate to the direct primitive vectors $\boldsymbol{a}_j$ of the original lattice with the following equation:

$$\boldsymbol{e}_i^* \boldsymbol{e}_j = 2\pi\delta_{i,j} \tag{2.3}$$

We can regard equation (2.3) as a second definition of the reciprocal lattice.

It can be proven that the reciprocal lattice of the reciprocal lattice is just the original lattice. In this context, the original Bravais lattice is often called the *direct lattice*.

First Brillouin zone. The *first Brillouin zone* around a lattice point of the reciprocal lattice consist of the region of space that is closer to that point than to any other point. It has the full point-symmetry of the reciprocal lattice, and it is the most common choice for a unit cell in the reciprocal lattice (the same concept can be defined for the direct lattice, and it is called the *Wigner-Seitz primitive cell*).

2.1.3 The independent electron approximation

The problem of electrons in solids is in principle a many-body problem, for which there most probably is no analytical solution. In the independent electron approximation, we forget about the electron-electron interactions. This greatly facilitates the task, because it means that we only have to solve a one-electron problem, which is the same for every electron in the crystal. The electron-nuclei interactions are represented by an effective potential $U(\boldsymbol{r})$. The one-electron time-independent Schrödinger equation is:

$$H\Psi(\boldsymbol{r}) = \left[-\frac{\hbar^2}{2m}\nabla^2 + U(\boldsymbol{r})\right]\Psi(\boldsymbol{r}) = \epsilon\Psi(\boldsymbol{r}) \tag{2.4}$$

The ground state of the system is obtained by filling the energy eigenstates from the lowest one up, until there is no electrons left. The total energy of the system is then the sum of all energies.

2.1.4 Bloch's theorem

It is sensible to assume the potential $U(\boldsymbol{r})$ to have the same translational symmetry as the crystal. This means that, being $\boldsymbol{R}$ a basis vector of the Bravais lattice:

$$U(\boldsymbol{r}+\boldsymbol{R}) = U(\boldsymbol{r}) \tag{2.5}$$

Bloch's theorem. *Bloch's theorem* is an extremely important theorem in condensed matter physics, and it states the following: solutions to the Schrödinger equation in a periodic potential take the form of a plane wave modulated by a periodic function. In other words, solutions $\Psi(\boldsymbol{r})$ must take the form:

$$\psi(\boldsymbol{r}) = e^{i\boldsymbol{k}\cdot\boldsymbol{r}}u(\boldsymbol{r}) \qquad u(\boldsymbol{r}+\boldsymbol{R}) = u(\boldsymbol{r}) \tag{2.6}$$

$u(\boldsymbol{r})$ is a function with the same periodicity as the lattice (and the potential), and it is often called *Bloch wave* in the literature.

2.1.5 Born-von Karman boundary conditions

The whole idea of tight-binding models, as we are going to see in the next section, is that the wave function of the electron is localized around the lattice sites, so that for the part localized around a lattice site, the effects of the neighboring atoms vanish at large distances.

From that perspective, we do not expect that the boundary conditions are of physical significance for the atoms in the bulk of the system, and we expect the same results for different boundary conditions for big enough systems.

The most convenient choice are the periodic boundary conditions, also called the *Born-von Karman boundary conditions*. We can express them as:

$$\Psi(\boldsymbol{r} + N_i\boldsymbol{e}_i) = \Psi(\boldsymbol{r}) \tag{2.7}$$

$N = \prod_{i=1}^{m} N_i$ being the number of unit cells that make the crystal. This boundary condition limits the possible values of $\mathbf{k}$:

$$\begin{gathered}\Psi(\boldsymbol{r} + N_i\boldsymbol{e}_i) = u(\boldsymbol{r} + \boldsymbol{N_i e_i})e^{i\boldsymbol{k}(\boldsymbol{r}+N_i\boldsymbol{e}_i)} = u(\boldsymbol{r})e^{i\boldsymbol{k}\cdot\boldsymbol{r}}e^{iN_i\boldsymbol{k}\cdot\boldsymbol{e}_i} = \Psi(\boldsymbol{r}) \\ e^{iN_i\boldsymbol{k}\boldsymbol{e}_i} = 1\end{gathered} \tag{2.8}$$

So the allowed Bloch wave vectors are:

$$\boldsymbol{k} = \sum_i \frac{n_i}{N_i}\boldsymbol{e}_i \tag{2.9}$$

It is trivial to check that there are N allowed $\mathbf{k}$-vectors in the unit cell of the reciprocal lattice. So the of set possible vectors is discrete, but for any reasonable values of N is extremely dense.

This boundary conditions are of course not adequate to study the physics near the edges of the crystal, so we must bear in mind that the results following from these constraints are valid only for the bulk.

2.1.6 The electronic band structure

For each vector $\boldsymbol{k}$ there will be a family of solutions, with discretely spaced eigenvalues. We are going to label these with the *band index* n.

An important result of band theory is that the dispersion relations are periodic functions in momentum space, with the periodicity of the reciprocal lattice. On the other hand, the wave functions for different values of $\boldsymbol{k}$ related by a reciprocal lattice vector represent the same state, so they can differ by a phase. One usually takes them to be equal, which is known as the *periodical gauge condition* [1]. In summary:

$$\begin{aligned} \Psi^n_{k+K}(r) &= \Psi^n_k(r) \\ \epsilon^n_{k+K} &= \epsilon^n_k \end{aligned} \tag{2.10}$$

This implies that it is enough to solve the problem for one unit cell, usually the first Brillouin zone. Even if the allowed $\boldsymbol{k}$ are discrete, the dispersion relations can be described as a family of continuous functions:

$$\{\epsilon^n(\boldsymbol{k})\}_{n=1,\dots,m} \tag{2.11}$$

These functions are often referred to as the *electronic energy bands*, and they together form the *electronic band structure* of the crystal. For a system with m atoms per unit site we will have m energy levels, and we can call it a *m-band system* [2].

The ground state of the N electron system is constructed by occupying the energy bands form the lowest one up. Two distinct types of configurations can result:

1. Insulators. A certain number of bands is completely filled, while all others remain empty. There is an energy gap between the top of the highest occupied band (also called *conducting band*) and the bottom of the lowest empty band (also called *valence band*). For band gaps much bigger than k_bT, solids are found to be electrical *insulators*. For band gaps comparable to k_bT, the solid is known as a *semiconductor*.

2. Conductors. A number of bands might be partially filled. This means that there is no band gap between the valence and conducting bands. Materials with this property are found to be electrical *conductors*.

2.2 Tigh-binding models

Tight-binding models are simple toy models that effectively describe the motion of electrons in solids. In a tight-binding model, the spectrum of possible states for an electron is discrete, and these are the orbitals localized at each site of the lattice.

A nice way to describe these models is by making use of the second quantization formalism that is going to be explained in the following section 2.2.1. The kinetic energy comes from the hoppings of electrons from one site to another, and it will be introduced in the hamiltonian with the help of the hopping operator. The potential energy comes from the on-site energy of the electrons in the orbitals.

In tight-binding models, the contribution to the energy of the hoppings becomes negligible when increasing the distance. That is why, in these toy-models, only the hoppings between first, sometimes second, and rarely third or fourth neighbours are usually considered.

2.2.1 Second quantization formalism

The most natural way to describe the state of a many-body system made of indistinguishable-particles is with *second quantization formalism*, also referred to as *occupation number representation*. The state ket is represented in the occupation number basis:

$$|\psi\rangle = |n_1, n_2, ..., n_N\rangle \tag{2.12}$$

where n_i is the number of particles in state i, and there are N possible states for a fermion. These kets "live" in Fock space (just as wave-functions live in Hilbert space). We don't specify which particle is in which state, only count the number of particles in each state, which makes the particles indistinguishable automatically [3].

Since we are dealing with fermions, occupation numbers have only two possible values: $n_i = 0$ or $n_i = 1$.

Fermionic creation and annihilation operators. The creation operator $c_i^\dagger$ and the annihilation operator c_i for fermions are defined as:

$$\{c_i, c_j^\dagger\} = \delta_{i,j} \tag{2.13}$$

$$\begin{aligned} c_i^\dagger |n_1, ..., n_i = 0, ..., n_N\rangle &= |n_1, ..., n_i = 1, ..., n_N\rangle \quad c_i^\dagger |n_1, ..., n_i = 1, ..., n_N\rangle = 0 \\ c_i |n_1, ..., n_i = 1, ..., n_N\rangle &= |n_1, ..., n_i = 0, ..., n_N\rangle \quad c_i |n_1, ..., n_i = 0, ..., n_N\rangle = 0 \end{aligned} \tag{2.14}$$

Anticommutation relation (2.13) ensures that the state is antisymmetric (since it is describing fermions).

The ground state. The state where all occupation numbers are equal to zero is the ground state:

$$|G\rangle = |0, 0, ..., 0\rangle \tag{2.15}$$

All other states can be constructed by acting on the ground state with the creation and annihilation operators.

Hopping operator. Operator $c_i^\dagger c_j$ annihilates a fermion in state i and creates another one in state j:

$$\begin{aligned} c_i^\dagger c_j \left|n_1, ..., n_i = 0, ..., n_j = 1, ..., n_N\right\rangle &= c_i^\dagger \left|n_1, ..., n_i = 0, ..., n_j = 0, ..., n_N\right\rangle \\ &= \left|n_1, ..., n_i = 1, ..., n_j = 0, ..., n_N\right\rangle \end{aligned} \tag{2.16}$$

If in the initial state $n_i = 1$ or $n_j = 0$, the result is just 0. We can interpret that this operation describes the hopping of an electron from one state to another. The hermitian conjugate of $c_i^\dagger c_j$ is just $c_j^\dagger c_i$, which describes a hopping between the same states, but in the opposite direction.

Particle number operator. The effect of operator $c_i^\dagger c_i$ in a ket:

$$\begin{aligned} &c_i^\dagger c_i \left|n_1, ..., n_i = 0, ..., n_N\right\rangle = 0 \\ &c_i^\dagger c_i \left|n_1, ..., n_i = 1, ..., n_N\right\rangle = c_i \left|n_1, ..., n_i = 0, ..., n_N\right\rangle = \left|n_1, ..., n_i = 1, ..., n_N\right\rangle \end{aligned} \tag{2.17}$$

We can define a particle number operator $\mathcal{N}$, so that any ket is its eigenvector and the eigenvalue gives the total number of fermions. If our system is composed of N fermions:

$$\mathcal{N} = \sum_i c_i c_i^\dagger \qquad \mathcal{N}\left|\Psi\right\rangle = N\left|\Psi\right\rangle \tag{2.18}$$

2.2.2 Position basis representation

For the purpose of this work we only need to consider tight-binding models with one state per spacial site, which really means that only one atomic orbital is involved in the dynamics of the system. We can express the state of the system, making use of the second quantization representation, in terms of the number of particles at each site of the lattice.

Notation. Since we are only going to use the second quantization basis to describe a single electron state, it is convenient to ease the notation. If n_j refers to the occupation number of site α of the unit given by lattice vector $\boldsymbol{R}$, from now on I will write:

$$\left|x_{\boldsymbol{R}}^\alpha\right\rangle = \left|n_1 = 0, n_2 = 0, ..., n_j = 1, ..., n_N = 0\right\rangle \tag{2.19}$$

It follows that:

$$c_{\boldsymbol{R}}^\alpha \left|G\right\rangle = \left|x_{\boldsymbol{R}}^\alpha\right\rangle \tag{2.20}$$

For the operators, in the case for a diatomic system with atoms in sites $\boldsymbol{r}_a$ and $\boldsymbol{r}_b$, we simplify the notation even more and use:

$$a_{\boldsymbol{R}} = c_{\boldsymbol{R}}^a \qquad b_{\boldsymbol{R}} = c_{\boldsymbol{R}}^b \tag{2.21}$$

2.2.3 Momentum basis representation

We can also use the occupation number representation to express the state in terms of the number of particles containing different momenta (n_i refers to the number of particles with momentum $\boldsymbol{k}_i$) [4]. The ket describing the one electron state would be $\left|\boldsymbol{k}\right\rangle$, so that:

$$c_{\boldsymbol{k}}^\dagger \left|G\right\rangle = \left|\boldsymbol{k}\right\rangle \tag{2.22}$$

$c_{\boldsymbol{k}}^\dagger$ is the creation operator in momentum space. $\left|\boldsymbol{k}\right\rangle$ is ain eigenstate of the lattice momentum, and its wavefunction is:

$$\left\langle \boldsymbol{r}|\boldsymbol{k}\right\rangle = \frac{1}{\sqrt{N}} e^{i\boldsymbol{k}\cdot\boldsymbol{r}} \tag{2.23}$$

2.2.4 Relationship between the two representations

The two representations are related by a discrete Fourier transformation:

$$\begin{aligned} c_{\boldsymbol{R}}^{\alpha\,\dagger} &= \frac{1}{\sqrt{N}} \sum_{\boldsymbol{k}} c_{\boldsymbol{k}}^{\alpha\dagger} e^{-i\boldsymbol{k}(\boldsymbol{R}+\boldsymbol{r}_\alpha)} \\ c_{\boldsymbol{R}}^{\alpha} &= \frac{1}{\sqrt{N}} \sum_{\boldsymbol{k}} c_{\boldsymbol{k}}^{\alpha} e^{i\boldsymbol{k}(\boldsymbol{R}_+\boldsymbol{r}_\alpha)} \end{aligned} \tag{2.24}$$

One can arrive to that conclusion expanding $|x_{\boldsymbol{R}}^{\alpha}\rangle$ as $|x_{\boldsymbol{R}}^{\alpha}\rangle = \sum_{\boldsymbol{k}} \langle \boldsymbol{k}|x_{\boldsymbol{R}}^{\alpha}\rangle\, |\boldsymbol{k}\rangle$, and using identities (2.20) and (2.22) plus the expression for wave function (2.23). The anti-transformations result in:

$$\begin{aligned} c_{\boldsymbol{k}}^{\alpha\dagger} &= \frac{1}{\sqrt{N}} \sum_{\boldsymbol{R}} c_{\boldsymbol{R}}^{\alpha\,\dagger} e^{i\boldsymbol{k}(\boldsymbol{R}+\boldsymbol{r}_\alpha)} \\ c_{\boldsymbol{k}}^{\alpha} &= \frac{1}{\sqrt{N}} \sum_{\boldsymbol{R}} c_{\boldsymbol{R}}^{\alpha} e^{-i\boldsymbol{k}(\boldsymbol{R}_+\boldsymbol{r}_\alpha)} \end{aligned} \tag{2.25}$$

One useful identity. Let us consider the case for a diatomic system and use notation (2.21). The following operator will appear in the tight-binding hamiltonian, and it will be useful to transform it into k-space.

$$\sum_{\boldsymbol{R}} a_{\boldsymbol{R}}^{\dagger} b_{\boldsymbol{R}'} = \sum_{\boldsymbol{k}} a_{\boldsymbol{k}}^{\dagger} b_{\boldsymbol{k}} e^{i\boldsymbol{k}(\boldsymbol{R}'+\boldsymbol{r}_b-\boldsymbol{R}-\boldsymbol{r}_a)} \tag{2.26}$$

In k-space, hoppings from b to a result in a term in the hamiltonian of the same form but multiplied by a phase factor, determined by how far the electron hop is. Proving the above expression is trivial knowing that $\frac{1}{N}\sum_{\boldsymbol{R}} e^{i\boldsymbol{R}(\boldsymbol{k}-\boldsymbol{k}')} = \delta_{\boldsymbol{k},\boldsymbol{k}'}$.

2.2.5 Expansion of the Bloch-like wave function

Solutions to the Schrödinger equation can be expanded into a basis $\left\{\left|\chi_\alpha^{\boldsymbol{k}}\right\rangle\right\}$:

$$\left|\chi_\alpha^{\boldsymbol{k}}\right\rangle = \sum_{\boldsymbol{R}} e^{i\boldsymbol{k}(\boldsymbol{R}+\boldsymbol{r}_\alpha)} \left|x_{\boldsymbol{R}}^{\alpha}\right\rangle \tag{2.27}$$

$$|\Psi_{\boldsymbol{k}}\rangle = \sum_{\alpha} C_{\boldsymbol{k}}^{\alpha} \left|\chi_{\boldsymbol{k}}^{\alpha}\right\rangle = \sum_{\boldsymbol{R},\alpha} C_{\boldsymbol{k}}^{\alpha} e^{i\boldsymbol{k}(\boldsymbol{R}+\boldsymbol{r}_\alpha)} \left|x_{\boldsymbol{R}}^{\alpha}\right\rangle \tag{2.28}$$

$$C_{\boldsymbol{k}+\boldsymbol{K}}^{\alpha} = C_{\boldsymbol{k}}^{\alpha} \tag{2.29}$$

Because of the periodic gauge, condition (2.29) must hold. For each band, there are m coefficients ($\alpha = 1, ..., m$) for a vector $\boldsymbol{k}$. These coefficients can be regarded as the discrete version of the Bloch waves $u_k^n(\boldsymbol{r})$.

2.2.6 Tight-binding hamiltonian in k-space

Performing a Fourier transformation of the hamiltonian H will be of extreme utility. It will be part of the procedure to get to the family of dispersion relations. For a m-band model, we will always arrive at an expression of this sort:

$$H = \sum_k \begin{pmatrix} c_k^{1\dagger} & c_k^{2\dagger} & ... & c_k^{m\dagger} \end{pmatrix} \mathcal{H}_k \begin{pmatrix} c_k^1 \\ c_k^2 \\ ... \\ c_k^m \end{pmatrix} \tag{2.30}$$

where c_k^α and $c_k^{\alpha\dagger}$ $\alpha = 1, 2, .., m$ come from the Fourier transformation of the creation/annihilation operators for each site of the unit cell (e.g. for a 2-band system c_k^1=a_k and c_k^2=b_k). This process is going to be made clear in chapter 3, where we implement the tight-binding approximation to study Haldane's model.

The $m \times m$ matrix $\mathcal{H}_k$ is the *Kernel* of the hamiltonian, or also often just called the hamiltonian. It has the same symmetries oft the hamiltonian and contains all useful information [5]. The utility of this transformation lies in the eigenvalues and eigenvectors of $\mathcal{H}_k$. For simplicity, from now on I will consider the case of a 2-band system.

Eigenvalues of $\mathcal{H}(\boldsymbol{k})$. One can always find an unitary matrix $U_{\boldsymbol{k}}$ that diagonalizes $\mathcal{H}_{\boldsymbol{k}}$:

$$U_{\boldsymbol{k}} = \begin{pmatrix} u^c_{a,\boldsymbol{k}} & u^d_{a,\boldsymbol{k}} \\ u^c_{b,\boldsymbol{k}} & u^d_{b,\boldsymbol{k}} \end{pmatrix} \longrightarrow U_{\boldsymbol{k}}^\dagger \mathcal{H} U_{\boldsymbol{k}} = \begin{pmatrix} \epsilon^c_{\boldsymbol{k}} & 0 \\ 0 & \epsilon^d_{\boldsymbol{k}} \end{pmatrix} \tag{2.31}$$

so that ϵ_c and ϵ_d are the eigenvalues of $\mathcal{H}$, and the corresponding eigenvectors are:

$$\mathcal{H}_{\boldsymbol{k}} \begin{pmatrix} u^c_{a,\boldsymbol{k}} \\ u^c_{b,\boldsymbol{k}} \end{pmatrix} = \epsilon^c_{\boldsymbol{k}} \begin{pmatrix} u^c_{a,\boldsymbol{k}} \\ u^c_{b,\boldsymbol{k}} \end{pmatrix} \quad \mathcal{H} \begin{pmatrix} u^d_{a,\boldsymbol{k}} \\ u^d_{b,\boldsymbol{k}} \end{pmatrix} = \epsilon^d_{\boldsymbol{k}} \begin{pmatrix} u^d_{a,\boldsymbol{k}} \\ u^d_{b,\boldsymbol{k}} \end{pmatrix} \tag{2.32}$$

Let us define two new operators (indicating the k-dependace again):

$$\begin{pmatrix} c_{\boldsymbol{k}} \\ d_{\boldsymbol{k}} \end{pmatrix} = U_{\boldsymbol{k}}^\dagger \begin{pmatrix} a_{\boldsymbol{k}} \\ b_{\boldsymbol{k}} \end{pmatrix} \qquad \begin{pmatrix} c^\dagger_{\boldsymbol{k}} & d^\dagger_{\boldsymbol{k}} \end{pmatrix} = \begin{pmatrix} a^\dagger_{\boldsymbol{k}} & b^\dagger_{\boldsymbol{k}} \end{pmatrix} U_{\boldsymbol{k}} \tag{2.33}$$

We can then rewrite the hamiltonian :

$$\begin{aligned} H = \sum_{\boldsymbol{k}} \begin{pmatrix} a^\dagger_{\boldsymbol{k}} & b^\dagger_{\boldsymbol{k}} \end{pmatrix} U_{\boldsymbol{k}} \begin{pmatrix} \epsilon^c_{\boldsymbol{k}} & 0 \\ 0 & \epsilon^d_{\boldsymbol{k}} \end{pmatrix} U_{\boldsymbol{k}}^\dagger \begin{pmatrix} a_{\boldsymbol{k}} \\ b_{\boldsymbol{k}} \end{pmatrix} &= \sum_{\boldsymbol{k}} \begin{pmatrix} c^\dagger_{\boldsymbol{k}} & d^\dagger_{\boldsymbol{k}} \end{pmatrix} \begin{pmatrix} \epsilon^c_{\boldsymbol{k}} & 0 \\ 0 & \epsilon^d_{\boldsymbol{k}} \end{pmatrix} \begin{pmatrix} c_{\boldsymbol{k}} \\ d_{\boldsymbol{k}} \end{pmatrix} \\ &= \sum_{\boldsymbol{k}} \epsilon^c_{\boldsymbol{k}} c^\dagger_{\boldsymbol{k}} c_{\boldsymbol{k}} + \sum_{\boldsymbol{k}} \epsilon^d_{\boldsymbol{k}} d^\dagger_{\boldsymbol{k}} d_{\boldsymbol{k}} \end{aligned} \tag{2.34}$$

The significance of the eigenvalues is clear if we compare this result to the expression for the energy:

$$E = \sum_{\boldsymbol{k},n} \epsilon_{\boldsymbol{k},n} n_{\boldsymbol{k},n} = \sum_{\boldsymbol{k}} e_1(\boldsymbol{k}) n_1(\boldsymbol{k}) + \sum_{\boldsymbol{k}} \epsilon_2(\boldsymbol{k}) n_2(\boldsymbol{k}) + ... \tag{2.35}$$

Conclusion: eigenvalues of $\mathcal{H}$ give us the dispersion relations.

Eigenvectors of $\boldsymbol{H(k)}$. $c_k^\dagger$ and $d_k^\dagger$ in equation (2.34) must be the creation operators for the Bloch-like eigenfunctions. Let us examine $c_k^\dagger$ (the same logic can be applied to $d_k^\dagger$):

$$c_{\boldsymbol{k}}^\dagger = u_a^c\, a_{\boldsymbol{k}}^\dagger + u_b^c\, b_{\boldsymbol{k}}^\dagger \tag{2.36}$$

Since $a_{\boldsymbol{k}}^\dagger$ and $b_{\boldsymbol{k}}^\dagger$ create plane waves, it is clear that the coefficients must be the discrete Bloch waves. In fact, if we act on the ground state with operator $c_{\boldsymbol{k}}^\dagger$, it is easy to see that we obtain the same expansion as in section 2.2.5. Therefore, we can identify coefficients u_α^n (where n is the band index and α indicates the site) with the ones in equation (2.28). For every band:

$$u_{\alpha,\boldsymbol{k}} = C_{\boldsymbol{k}}^\alpha \tag{2.37}$$

Conclusion: eigenvectors of $\mathcal{H}$ give us the discrete Bloch waves.

2.2.7 Eigenvalues and eigenvectors for a 2-band model

We want to calculate the general expression for the eigenvectors and eigenvalues of a two-dimensional hamiltonian $\mathcal{H} = \mathcal{H}(k)$ (I will not write the k dependence explicitly). This matrix can be written as a linear combination of the Pauli matrices and the identity matrix, since these four form a basis in the space of complex hermitian 2 x 2 matrices.

$$\mathcal{H} = \mathcal{H}_0 \mathbb{1} + \mathcal{H}_x \sigma_x + \mathcal{H}_y \sigma_y + \mathcal{H}_z \sigma_z \tag{2.38}$$

So that:

$$\mathcal{H} = \begin{pmatrix} \mathcal{H}_{11} & \mathcal{H}_{12} \\ \mathcal{H}_{21} & \mathcal{H}_{22} \end{pmatrix} = \begin{pmatrix} \mathcal{H}_0 + \mathcal{H}_z & \mathcal{H}_x - i\mathcal{H}_y \\ \mathcal{H}_x + i\mathcal{H}_y & \mathcal{H}_0 - \mathcal{H}_z \end{pmatrix}$$

$$\begin{aligned} \mathcal{H}_0 &= \frac{\mathcal{H}_{11} + \mathcal{H}_{22}}{2} \qquad & \mathcal{H}_z &= \frac{\mathcal{H}_{11} - \mathcal{H}_{22}}{2} \\ \mathcal{H}_x &= Re[\mathcal{H}_{21}] & \mathcal{H}_y &= Im[\mathcal{H}_{21}] \end{aligned} \tag{2.39}$$

Computing the eigenvalues and eigenvectors of $\mathcal{H}$ is straightforward. The eigenvalues are:

$$\begin{aligned} \epsilon^- &= \mathcal{H}_0 - |\vec{\mathcal{H}}| = \mathcal{H}_0 - \sqrt{\mathcal{H}_x^2 + \mathcal{H}_y^2 + \mathcal{H}_z^2} \\ \epsilon^+ &= \mathcal{H}_0 + |\vec{\mathcal{H}}| = \mathcal{H}_0 + \sqrt{\mathcal{H}_x^2 + \mathcal{H}_y^2 + \mathcal{H}_z^2} \end{aligned} \tag{2.40}$$

And the eigenvectors:

$$u^- = \begin{pmatrix} \mathcal{H}_z - |\vec{\mathcal{H}}| \\ \mathcal{H}_x + i\mathcal{H}_y \end{pmatrix} \qquad u^+ = \begin{pmatrix} \mathcal{H}_z + |\vec{\mathcal{H}}| \\ \mathcal{H}_x + i\mathcal{H}_y \end{pmatrix} \tag{2.41}$$

Results (2.40) and (2.41) will be useful in chapter 3.

2.3 Topology in band theory

The aim of this section is to present some basic concepts related to topology in the context of band theory. These are going to be needed to understand the particular case of Haldane's model in the following chapter.

2.3.1 Gauge symmetry and the Berry connection

Apart from the global U(1) symmetry from phase invariance of quantum mechanics, there is an additional local symmetry in tight-binding systems, and in band-theory in general. Bloch-waves are invariant under a local phase shift in the momentum space [6]:

$$\Psi_{\boldsymbol{k}} \longrightarrow e^{i\phi(\boldsymbol{k})}\Psi_{\boldsymbol{k}} \tag{2.42}$$

Both waves are the same eigenstate. This invites the definition of a potential and a gauge transformation, in the same way as in electromagnetic theory.

Such potential, analogous to the magnetic vector potential, is the *Berry connection*, and it is gauge dependent. The gauge invariant magnitude analogous to the magnetic field is called the *Berry curvature*.

For every eigenstate $\Psi^n_{\boldsymbol{k}}(\boldsymbol{r}) = u^n_{\boldsymbol{k}}(\boldsymbol{r})e^{i\boldsymbol{k}\cdot\boldsymbol{r}}$, n being the band index, the following definitions hold:

Berry connection:

$$\boldsymbol{\mathcal{A}}_n(\boldsymbol{k}) = -i < u^n_{\boldsymbol{k}}|\boldsymbol{\nabla}_{\boldsymbol{k}}|u^n_{\boldsymbol{k}} > \tag{2.43}$$

Berry curvature:

$$\boldsymbol{\mathcal{F}}_n(\boldsymbol{k}) = \boldsymbol{\nabla}_{\boldsymbol{k}} \times \boldsymbol{\mathcal{A}}_n(\boldsymbol{k}) = -i\epsilon_{ij}\left\langle u^i_{\boldsymbol{k}}\middle|u^j_{\boldsymbol{k}}\right\rangle \tag{2.44}$$

Gauge transform:

$$\begin{aligned} |u^n_{\boldsymbol{k}} > &\longrightarrow e^{i\phi_n(\boldsymbol{k})}|u^n_{\boldsymbol{k}} > \\ \boldsymbol{\mathcal{A}}_n(\boldsymbol{k}) &\longrightarrow \boldsymbol{\mathcal{A}}_n(\boldsymbol{k}) + \boldsymbol{\nabla}\phi_n(\boldsymbol{k}) \\ \boldsymbol{\mathcal{F}}_n(\boldsymbol{k}) &\longrightarrow \boldsymbol{\mathcal{F}}_n(\boldsymbol{k}) \end{aligned} \tag{2.45}$$

2.3.2 Topological invariants. Chern number

It can be proven that an integral of the Berry curvature (the *Berry flux*) over a closed 2D manifold is quantized:

$$\oiint \boldsymbol{\mathcal{F}}(\boldsymbol{k})d\boldsymbol{k} = 2\pi C \tag{2.46}$$

Moreover, it can be proven that it is a topological invariant: it gives the same result for closed manifolds that are topologically equivalent [7]. In simple terms, being topologically

equivalent means that one manifold can be transformed into the other by a continuous transformation, without causing or eliminating any holes. Mathematically, this transformation is called a homeomorphism.

Since the 2D Brillouin zone has periodic boundary conditions along x and y, it is a closed manifold, in particular, a torus. This means that:

$$\oiint_{BZ} \boldsymbol{\mathcal{F}} d\boldsymbol{k} = 2\pi C \tag{2.47}$$

For an insulator, the scalar magnitude C is called the **Chern number** or the **Topological index**.

$$C = \frac{1}{2\pi} \oiint \boldsymbol{\mathcal{F}} d\boldsymbol{k} \tag{2.48}$$

The calculation must be done for each one of the energy bands. It is a mathematical fact that the sum of all Chern number is equal to 0 (this implies that there cannot be one-band non-trivial insulators). These numbers define the topological phase of an insulator. On the other hand, the Chern number is only well defined for insulating systems, with no band-crossing.

2.3.3 Topological transitions and protected magnitudes

From the topological perspective, band structures are equivalent if they can be continuously deformed into one another without closing the energy gap, because under this transformation the topology of the system remains unchanged.

Even when the gap closes, a topological transition does not always occur. So band crossing is a necessary but not sufficient condition for a topological transition.

If a physical magnitude is topologically invariant (for example, if it is proportional to C), its value won't change even if we perturb a system, as long as we don't close the gap and trigger a topological transition. This makes such magnitudes very stable.

Example: Integer Quantum Hall Effect. The first and most famous example of this phenomenon is the quantization of the hall conductivity. In the integer quantum hall effect we have that:

$$\sigma_{xy} = \frac{e}{2\pi c^2} \oiint_{BZ} \boldsymbol{\mathcal{F}} d\boldsymbol{k} = \frac{e}{c^2} C \tag{2.49}$$

The experimental results show very clear platteaus in values $\sigma_{xy} = \frac{e}{c^2} n$ (where n is an integer) when it is meassured versus an increasing magnetic field. After arriving at result 2.49, one can qualitatively understand why: even if the hamiltonian and band structure change with the change in the magnetic field, σ_{xy} remains stable until the change is significant enough that bands cross and a topological transition occurs [8].

2.3.4 Topological insulators

Topological insulators have the surprising property of being insulators in the bulk, but metals near the boundary. The conducting edge states are topologically protected, and are stable as long as the system does not undergo a topological transition.

This study is limited to 2D insulators with broken time-reversal symmetry, which can be well characterized by the magnitude C. The spin degree of freedom is ignored since it does not play a role in the dynamics of the system. These are the simplest case of a topological insulator, and are often called *Chern insulators*.

In order to be a topological insulator a system must have $C \neq 0$. In that case, the edge states will appear in the finite system. On the other hand, we say an insulator is topologically trivial when $C = 0$ for all bands.

2.3.5 The role of time-reversal symmetry

Time reversal symmetry is of crucial importance for Chern insulators. Let τ be the operator of time-reversal. When acting on the wave vector $\boldsymbol{k}$, we have that:

$$\tau \boldsymbol{k} = -\boldsymbol{k} \tag{2.50}$$

One can imagine that the velocity changes sign when time changes sign, and so does the momentum. On the other hand, since τ is an anti-unitary operator, when acting on a wave function:

$$\tau u_{\boldsymbol{k}}(\boldsymbol{r}) = u^*_{-\boldsymbol{k}}(\boldsymbol{r}) \tag{2.51}$$

In bra-ket formalism, this implies that for a scalar multiplication:

$$\tau < u^a_{\boldsymbol{k}} | u^b_{\boldsymbol{k}} > = < u^b_{-\boldsymbol{k}} | u^a_{-\boldsymbol{k}} > \tag{2.52}$$

With these results we can examine the effects of τ on the Berry flux:

$$\begin{aligned} \tau \boldsymbol{\mathcal{F}}(\boldsymbol{k}) = -i\epsilon_{ij} \tau \left\langle u^i_{\boldsymbol{k}} \middle| u^j_{\boldsymbol{k}} \right\rangle = -i\epsilon_{ij} \left\langle u^j_{-\boldsymbol{k}} \middle| u_{-\boldsymbol{k}} i \right\rangle = \\ i\epsilon_{ji} \left\langle u^j_{-\boldsymbol{k}} \middle| u_{-\boldsymbol{k}} \right\rangle = -\boldsymbol{\mathcal{F}}(-\boldsymbol{k}) \end{aligned} \tag{2.53}$$

For a system with time reversal symmetry $\boldsymbol{\mathcal{F}}(\boldsymbol{k})$ is an odd function of $\boldsymbol{k}$ ($-\boldsymbol{\mathcal{F}}(-\boldsymbol{k}) = \boldsymbol{\mathcal{F}}(\boldsymbol{k})$). Integrating $\boldsymbol{\mathcal{F}}(\boldsymbol{k})$ in the Brillouin zone will give 0.

In conclusion, for a system with time reversal symmetry, $C = 0$. We will recall this fact in the analysis of Haldane's model in Chapter 3.

2.3.6 Interpreting singularities of Bloch waves.

The eigenvectors for a 2-dimensional hamiltonian were obtained in section 2.2.7 (I will indicate the $\boldsymbol{k}$-dependence explicitly):

$$u^-(\boldsymbol{k}) = \begin{pmatrix} \mathcal{H}_z(\boldsymbol{k}) - |\vec{\mathcal{H}}(\boldsymbol{k})| \\ \mathcal{H}_x(\boldsymbol{k}) + i\mathcal{H}_y(\boldsymbol{k}) \end{pmatrix} \qquad u^+(\boldsymbol{k}) = \begin{pmatrix} \mathcal{H}_z(\boldsymbol{k}) + |\vec{\mathcal{H}}(\boldsymbol{k})| \\ \mathcal{H}_x(\boldsymbol{k}) + i\mathcal{H}_y(\boldsymbol{k}) \end{pmatrix} \tag{2.54}$$

Let us now focus on the lower band (eigenvecotr $u^-(\boldsymbol{k})$). Suppose there is a value of $\boldsymbol{k}$ for which $\mathcal{H}_x(\boldsymbol{k}) = \mathcal{H}_y(\boldsymbol{k}) = 0$. If $\mathcal{H}_z > 0$, $u^-(\boldsymbol{k})$ is singular at that point. Therefore, the above expression for u^- does not give an useful Bloch wave to calculate quantities such as the Berry flux for those values of $\boldsymbol{k}$. But eigenvectors are not unique, and one could of course also choose any v^- proportional to u^-, for example:

$$v^-(\boldsymbol{k}) = \begin{pmatrix} -\mathcal{H}_x(\boldsymbol{k}) + i\mathcal{H}_y(\boldsymbol{k}) \\ \mathcal{H}_z(\boldsymbol{k}) + |\vec{\mathcal{H}}(\boldsymbol{k})| \end{pmatrix} \tag{2.55}$$

This is, in fact, a gauge transformation (equation 2.45) where $e^{i\theta(\boldsymbol{k})} = \frac{\frac{\mathcal{H}_z(\boldsymbol{k})+|\vec{\mathcal{H}}(\boldsymbol{k})|}{\mathcal{H}_x(\boldsymbol{k})+i\mathcal{H}_y(\boldsymbol{k})}}{\left|\frac{\mathcal{H}_z(\boldsymbol{k})+|\vec{\mathcal{H}}(\boldsymbol{k})|}{\mathcal{H}_x(\boldsymbol{k})+i\mathcal{H}_y(\boldsymbol{k})}\right|}$ and Berry curvature $\mathcal{F}(\boldsymbol{k})$ is unchanged.

The new vector presents the same problem in the case for $\mathcal{H}_x(\boldsymbol{k}) = \mathcal{H}_y(\boldsymbol{k}) = 0$ and $\mathcal{H}_z(\boldsymbol{k}) < 0$. It seems that the singularity has been avoided just by using a different gauge (so it was not a *real* singularity). But, if there are different regions in the Brillouin zone, one where $\mathcal{H}_z(\boldsymbol{k}) < 0$ and other where $\mathcal{H}_z(\boldsymbol{k}) > 0$, no matter what gauge we use, the singularity is inevitable.

If this happens, when calculating the Berry flux (and C), the Brillouin zone has to be separated into two regions, in order to use a different expression for the Bloch wave in each region. If one solves the integrals analytically, the mathematical result is the following: $C = -1$ for the lower band. Repeating the same analysis for the upper band, one gets $C = 1$ for the upper band. If there are no singularities, the result is C=0 : the insulator is trivial. When applicable, this results provide an easy way to know if the topological phase of a system is trivial or not, without having to compute the integrals [9].

Chapter 3

A case study: Haldane's model

In 1987, F. Duncan Haldane presented a toy model for graphene that featured topologically distinct phases [10]. The model is based on breaking time-reversal symmetry, through the introduction of complex next-nearest-neighbour hopping terms. Inversion symmetry is also broken, with an energy offset between neighbouring sites.

The aim of this chapter is to solve different tight binding models for an infinite honeycomb lattice, both analytically and computationally, and then put these together to arrive at the topological nontrivial system that Haldane proposed. In addition, the case for a finite system will be solved computationally, and the topologically protected conducting edge states will be deduced.

3.1 Computational tool: the PythTB package

The *Python Tight Binding* (PythTB) package is an open access software package providing a Python implementation of the tight-binding approximation. It can be used to construct and solve tight-binding models of the electronic structure, and it is rich with features for computing Berry phases and related properties, such as the Berry flux [11].

The package is intended for research as well as pedagogical purposes, because of its easy implementation. On the downside, it is not a computationally efficient platform when applied to large systems requiring heavy computation. Nevertheless, for the purpose of this chapter, the PythTB package is the ideal computational tool.

There are many examples of the usage of the package provided by the authors in the PythTB web page. A pair of these examples have been the starting point for the code used in this chapter.

The package has been employed with three purposes: the visualization of the tight binding models, to solve for the energy eigenstates and eigenvectors of the tight-binding hamiltonian, and to calculate the Berry flux. This package, together with the well known *Matplotlib* Python package for creating visualizations, have been the tools used to create all the images in this document.

3.2 The honeycomb lattice

Graphene has a two-dimensional honeycomb geometry. This is a hexagonal Bravais lattice with two sites per unit cell, and the corresponding plane symmetry group is p6mm.

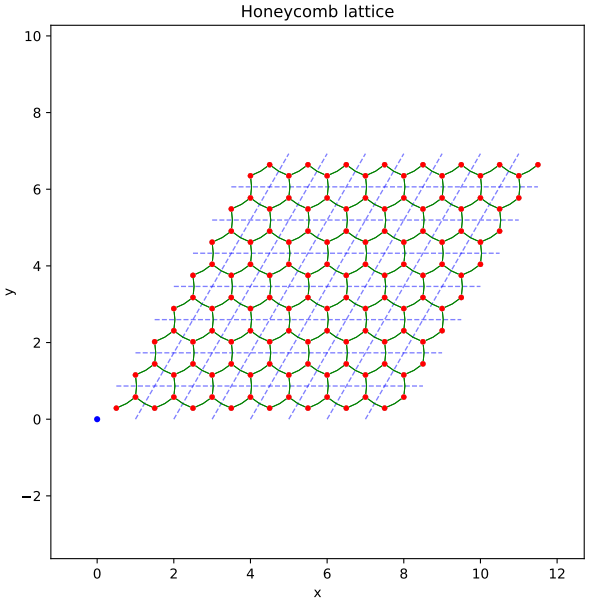

Figure 3.1: Visualization of the honeycomb lattice. Nearest neighbouring atoms are connected by green lines. The hexagonal Bravais lattice is drawn with blue dashed lines, and the blue point indicates the origin.

The basis vectors for the lattice, given in an orthonormal basis, are:

$$\begin{aligned} \boldsymbol{e_1} &= (a, 0) \\ \boldsymbol{e_2} &= \left(\frac{a}{2}, \frac{\sqrt{3}a}{2}\right) \end{aligned} \tag{3.1}$$

Where a is the distance between the centers of adjacent cells. From now on, we take a=1. Positions of sites A and B, in terms of the basis vectors $\boldsymbol{e_1}, \boldsymbol{e_2}$, are:

$$\begin{aligned} \boldsymbol{r}_a &= \left(\frac{1}{3}, \frac{1}{3}\right) \\ \boldsymbol{r}_b &= \left(\frac{2}{3}, \frac{2}{3}\right) \end{aligned} \tag{3.2}$$

I will use the following notation to refer to a specific site on the lattice: $A(v_1, v_2)$ or $B(v_1, v_2)$. The first letter indicates the type of site (A or B) and (v_1, v_2) are the coordinates of the unit cell where the site is in, with respect to the lattice basis vectors $\boldsymbol{e_1}$ and $\boldsymbol{e_2}$.

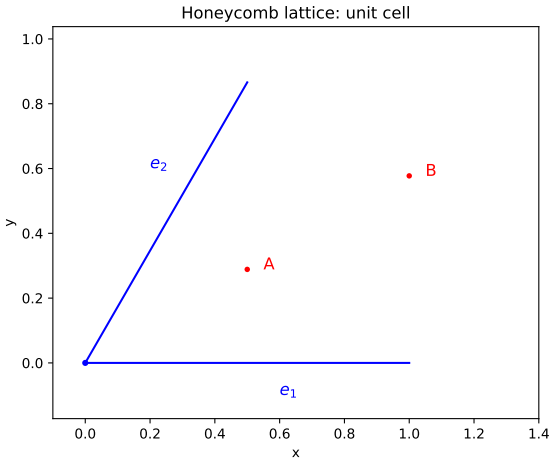

Figure 3.2: Unit cell of the honeycomb lattice. Basis vectors in blue, A and B sites in red.

The reciprocal lattice of the hexagonal lattice is another hexagonal lattice, tilted 30º (Figure 3.3). Basis vectors are:

$$\begin{aligned} \boldsymbol{e}_1^* &= 2\pi \left(1, -\frac{1}{\sqrt{3}}\right) \\ \boldsymbol{e}_2^* &= 2\pi \left(0, \frac{2}{\sqrt{3}}\right) \end{aligned} \tag{3.3}$$

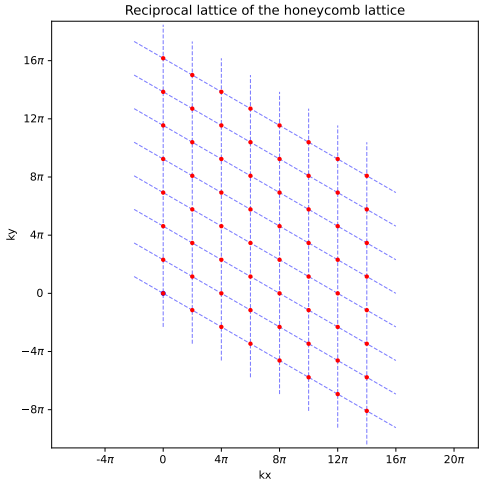

Figure 3.3: Visualization of the reciprocal lattice.

3.3 Honeycomb lattice with nearest neighbour hoppings

The first model that will be analyzed is a monatomic honeycomb lattice where electrons can only hop from one atom to its nearest neighbours (NN). The green lines in Figure 3.1 represent these hoppings. We assume that the hamiltonian is not spin dependant, in this and all models that are going to be studied.

Since atoms in site A and in site B are identical, all hoppings terms in this model have the same value $(-t)$. By inspection, we see we have three hoppings per unit cell (in reality, there are six, if one counts both hopping directions). In order to build the tight-binding hamiltonian, we sum the contributions to the energy of the three hoppings over all unit cells. Let us take these three hoppings: $A(0,0) \to B(0,0)$, $A(0,0) \to B(-1,0)$, $A(0,0) \to B(0,-1)$. Then, the hamiltonian can be written as:

$$H_{NN} = -t \sum_{\boldsymbol{R}} a^\dagger_{\boldsymbol{R}} b_{\boldsymbol{R}} - t \sum_{\boldsymbol{R}} a^\dagger_{\boldsymbol{R}} b_{\boldsymbol{R}-\boldsymbol{e_1}} - t \sum_{\boldsymbol{R}} a^\dagger_{\boldsymbol{R}} b_{\boldsymbol{R}-\boldsymbol{e_2}} + h.c. \tag{3.4}$$

The term *h.c.* means *Hermitian conjugate*. It is necessary for the hamiltonian to be hermitian, and it contains the hoppings in the opposite direction.

Since the system is monatomic, the on-site energy of each site is also the same. One can always take the origin at the total potential energy, that is why the potential energy is not included in equation (3.4). On the other hand, for systems with more than one type of atom, we cannot erase the different on-site energies from the hamiltonian.

In order to get the dispersion relations for the energy, we perform a Fourier transform to go to the momentum space, which results in:

$$\begin{aligned} H_{NN} &= -t \sum_{\boldsymbol{k}} a^\dagger_{\boldsymbol{k}} b_{\boldsymbol{k}} e^{i\boldsymbol{k}\cdot(\boldsymbol{r}_b - \boldsymbol{r}_a)} - t \sum_{\boldsymbol{k}} a^\dagger_{\boldsymbol{k}} b_{\boldsymbol{k}} e^{i\boldsymbol{k}\cdot(\boldsymbol{r}_b - \boldsymbol{r}_a - \boldsymbol{e}_1)} - t \sum_{\boldsymbol{k}} a^\dagger_{\boldsymbol{k}} b_{\boldsymbol{k}} e^{i\boldsymbol{k}\cdot(\boldsymbol{r}_b - \boldsymbol{r}_a - \boldsymbol{e}_2)} + h.c. \\ &= -t e^{i\boldsymbol{k}\cdot(\boldsymbol{r}_b - \boldsymbol{r}_a)} \left(\sum_{\boldsymbol{k}} a^\dagger_{\boldsymbol{k}} b_{\boldsymbol{k}} + \sum_{\boldsymbol{k}} a^\dagger_{\boldsymbol{k}} b_{\boldsymbol{k}} e^{-i\boldsymbol{k}\cdot\boldsymbol{e}_1} + \sum_{\boldsymbol{k}} a^\dagger_{\boldsymbol{k}} b_{\boldsymbol{k}} e^{-i\boldsymbol{k}\cdot\boldsymbol{e}_2} \right) + h.c. \end{aligned} \tag{3.5}$$

where I made use of result (2.26). Since the phase $e^{i\boldsymbol{k}\cdot(\boldsymbol{r}_b - \boldsymbol{r}_a)}$ will not affect the dispersion relations, can be ignored. We can manipulate this expression into the form (2.30), and obtain the kernel of the hamiltonian :

$$\begin{aligned} H_{NN} = -t \sum_{\boldsymbol{k}} a^\dagger_{\boldsymbol{k}} b_{\boldsymbol{k}} (1 + e^{-i\boldsymbol{k}\boldsymbol{e}_1} + e^{-i\boldsymbol{k}\boldsymbol{e}_2}) - t \sum_{\boldsymbol{k}} b^\dagger_{\boldsymbol{k}} a_{\boldsymbol{k}} (1 + e^{i\boldsymbol{k}\cdot\boldsymbol{e}_1} + e^{i\boldsymbol{k}\cdot\boldsymbol{e}_2}) = \\ \sum_{\boldsymbol{k}} \begin{pmatrix} a^\dagger_{\boldsymbol{k}} & b^\dagger_{\boldsymbol{k}} \end{pmatrix} \begin{pmatrix} 0 & -t(1 + e^{-i\boldsymbol{k}\cdot\boldsymbol{e}_1} + e^{-i\boldsymbol{k}\cdot\boldsymbol{e}_2}) \\ -t(1 + e^{i\boldsymbol{k}\boldsymbol{e}_1} + e^{i\boldsymbol{k}\cdot\boldsymbol{e}_2}) & 0 \end{pmatrix} \begin{pmatrix} a_{\boldsymbol{k}} \\ b_{\boldsymbol{k}} \end{pmatrix} \end{aligned}$$

$$\mathcal{H}_{NN} = \begin{pmatrix} 0 & \mathcal{H}_{12} \\ \mathcal{H}_{21} & 0 \end{pmatrix} = \begin{pmatrix} 0 & -t(1 + e^{-i\boldsymbol{k}\cdot\boldsymbol{e}_1} + e^{-i\boldsymbol{k}\cdot\boldsymbol{e}_2}) \\ -t(1 + e^{i\boldsymbol{k}\boldsymbol{e}_1} + e^{i\boldsymbol{k}\cdot\boldsymbol{e}_2}) & 0 \end{pmatrix} \tag{3.6}$$

In terms of the Pauli matrices, we can write it as:

$$\begin{gathered}\mathcal{H}_{NN} = \mathcal{H}_0\mathbb{1}+\mathcal{H}_x\sigma_x + \mathcal{H}_y\sigma_y + \mathcal{H}_z\sigma_z \\ \mathcal{H}_0 = \mathcal{H}_z = 0 \\ \mathcal{H}_x = Re[\mathcal{H}_{21}] = -\,t\,[1 + cos(\boldsymbol{k}\boldsymbol{e}_1) + cos(\boldsymbol{k}\boldsymbol{e}_2)] \\ \mathcal{H}_y = Im[\mathcal{H}_{21}] = t\,[sin(\boldsymbol{k}\boldsymbol{e}_1) + sin(\boldsymbol{k}\boldsymbol{e}_2)]\end{gathered} \tag{3.7}$$

This result will be used to make comparison with other models. The dispersion relations are given by the eigenvalues of $\mathcal{H}$:

$$\begin{aligned}\epsilon^{\pm} &= \pm\,|t|\sqrt{3 + 2cos(\boldsymbol{k}\cdot\boldsymbol{e}_1) + 2cos(\boldsymbol{k}\cdot\boldsymbol{e}_2) + 2cos(\boldsymbol{k}\cdot(\boldsymbol{e}_1 - \boldsymbol{e_2}))} \\ &= \pm|t|\sqrt{2 + 2cos(k_x) + 4cos(\frac{k_x}{2})cos(\frac{\sqrt{3}k_y}{2})}\end{aligned} \tag{3.8}$$

Figure 3.4a shows a surface plot of the energy bands. We can see that they touch at 6 points. These six points are actually two independent points in k-space, and their 4 symmetry related counterparts. Expressed in the reciprocal lattice basis $(\boldsymbol{e}_1^*, \boldsymbol{e}_2^*)$:

$$\begin{aligned}K &= \left(-\frac{1}{3}, \frac{1}{3}\right) \equiv \left(-\frac{1}{3}, -\frac{2}{3}\right) \equiv \left(\frac{2}{3}, \frac{1}{3}\right) \\ K' &= \left(\frac{1}{3}, -\frac{1}{3}\right) \equiv \left(\frac{1}{3}, \frac{2}{3}\right) \equiv \left(-\frac{2}{3}, -\frac{1}{3}\right)\end{aligned} \tag{3.9}$$

And expressed in an orthonormal basis:

$$\begin{aligned}K &= 2\pi\left(-\frac{1}{3}, \frac{1}{\sqrt{3}}\right) \equiv 2\pi\left(-\frac{1}{3}, -\frac{1}{\sqrt{3}}\right) \equiv 2\pi\left(\frac{2}{3}, 0\right) \\ K' &= 2\pi\left(\frac{1}{3}, -\frac{1}{\sqrt{3}}\right) \equiv 2\pi\left(\frac{1}{3}, \frac{1}{\sqrt{3}}\right) \equiv 2\pi\left(-\frac{2}{3}, 0\right)\end{aligned} \tag{3.10}$$

K and K' points are related by inversion symmetry. At these six points the energy is degenerate: equation (3.8) gives $\epsilon^- = \epsilon^+ = 0$. It is easy to check using the first expression of eq. (3.8) and the identity $\boldsymbol{e_i}\boldsymbol{e_j}^* = 2\pi\delta_{i,j}$:

$$\begin{aligned}k = K = \left(-\frac{1}{3}, \frac{1}{\sqrt{3}}\right) \longrightarrow \epsilon^{\pm} &= \pm\,|t|\sqrt{3 + 2cos(-\frac{2\pi}{3}) + 2cos(\frac{2\pi}{3}) + 2cos(\frac{4\pi}{3})} \\ &= \pm\,|t|\sqrt{3 + 4(-\frac{1}{2}) - \frac{1}{2}} = 0\end{aligned}$$

$$k = \vec{K'} = \left(\frac{1}{3}, -\frac{1}{\sqrt{3}}\right) \longrightarrow \epsilon^{\pm} = \pm\,|t|\sqrt{3 + 2cos(\frac{2\pi}{3}) + 2cos(-\frac{2\pi}{3}) + 2cos(-\frac{4\pi}{3})} = 0$$

Figure 3.4b shows the band structure over a path at k-space: form the origin (Γ) to K, from K to $M(\frac{1}{2}, \frac{1}{2})$, which is a saddle point, from M to K', and from K' back to the origin. It is clear that the two bands touch at the K and K' points.

Both figures have been created by solving the tight biding model computationally with the PythTB package, and the graphing the results.

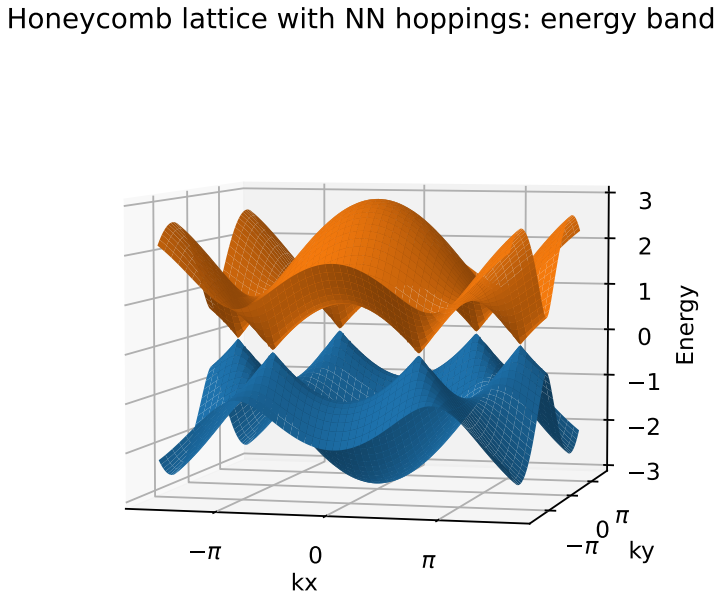

(a)

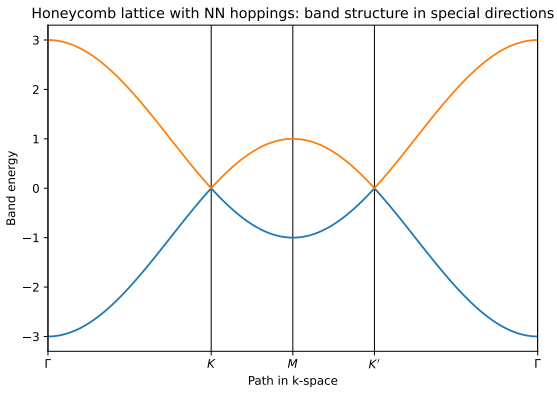

(b)

Figure 3.4: Electronic energy bands for a honeycomb lattice with nearest neighbour hoppings. $t = 1.0$.

If we apply this model to graphene, atoms in A and B sites are carbon atoms, connected to their three nearest neighbors by a σ-bond, and each atom introduces one electron to the valence band [12]. Since each band can hold two electrons of opposite spin, zero energy graphene is exactly half-filled: the valence band is completely filled while the conduction band is completely empty. The Fermi energy lies exactly at the intersection of the two bands. So, undoped graphene is a semi-metal, also often called a zero-gap semiconductor.

3.3.1 Dirac points and Dirac cones

The K and K' points are exactly the edges of the first Brillouin zone, which is a hexagon, and are often called *Dirac points*. Figure 3.5 illustrates the K and K' points on the reciprocal lattice.

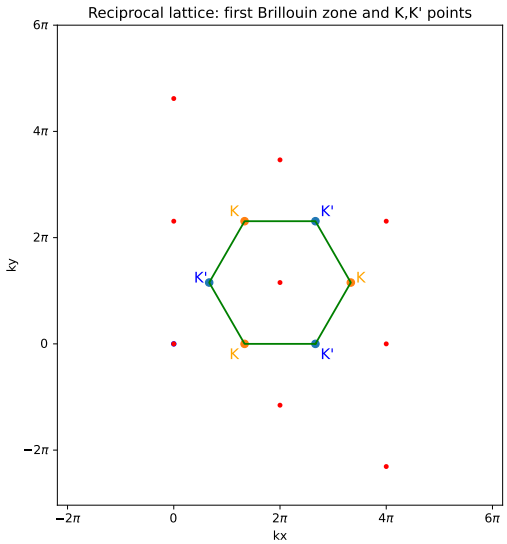

Figure 3.5: Visualization of K (orange) and K' (blue) points on the reciprocal lattice. The hexagonal first Brillouin zone is marked in green.

The name *Dirac point* comes from the fact that if we expand the expression for the energy (eq. (3.8)) near these points, we get a linear relation between the energy and the momentum: $\epsilon(\vec{K}+\vec{k}) \approx ck$. Electrons obey a "Dirac-like" equation, and behave as they were massles. If we zoom-in to a K or K' point, we can see the bands form a *Dirac cone* (Figure 3.6).

The Dirac points in the honeycomb lattice are stable as long as space inversion symmetry and time reversal symmetry are preserved. No matter how one perturbs the systems (e.g. adding longer-range hoppings), the Dirac point is always there as long as the two symmetries are preserved.

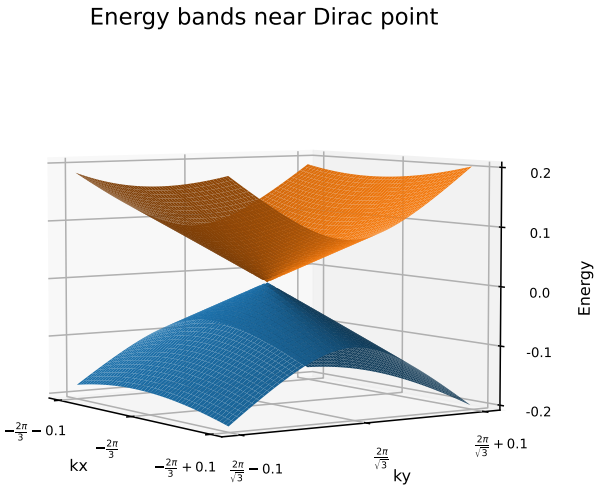

Figure 3.6: Surface plot of *Dirac cone*, centered at $K = 2\pi(-\frac{1}{3}, \frac{1}{\sqrt{3}})$.

This is because the only way to open a gap between the bands is by adding a σ_z type of term to the hamiltonian from eq. (3.6). Adding new terms to $\mathcal{H}_x$ and $\mathcal{H}_y$ only results in moving the Dirac points around, so they no longer lie in the corners of the first Brillouin zone, but they don't disappear.

Inversion symmetry enforces the relation:

$$\mathcal{H}(\boldsymbol{k}) = -\mathcal{H}(-\boldsymbol{k}) \longrightarrow \mathcal{H}_z(\boldsymbol{k}) = -\mathcal{H}_z(-\boldsymbol{k}) \tag{3.11}$$

On the other hand, time-reversal symmetry enforces the relation:

$$\mathcal{H}(\boldsymbol{k}) = \mathcal{H}^*(-\boldsymbol{k}) \longrightarrow \mathcal{H}_z(\boldsymbol{k}) = \mathcal{H}_z^*(-\boldsymbol{k}) = \mathcal{H}_z(-\boldsymbol{k}) \tag{3.12}$$

So, if both symmetries are fulfilled, $\mathcal{H}_z = 0$ is satisfied. The gap is not opened and Dirac points are maintained. We can also conclude that if $\mathcal{H}_z \neq 0$, at least one of the two symmetries has been broken.

3.4 Different on-site energies

Let us now consider the same honeycomb lattice as in the previous section, but assign a different potential energy to atoms in different sites. It is a requisite that atoms in site A and B are different, such that the surroundings of the two sites are not identical (this would make the on-site potentials also identical). We no longer have a monatomic system, so this toy model does not describe graphene.

Three examples of two-dimesional diatomic hexagonal materials are single layer BN, MoS_2 and $NbSe_2$ [13]. It is important to note that we no longer have inversion symmetry, so we expect a band-gap.

We can take the origin for the energy in the middle of the two potentials, so that the potential is equal to V for site A and $-V$ for site B. To the hamiltonian in equation (3.8), we have to add this new term:

$$H_{pot} = V \sum_{\boldsymbol{R}} a^\dagger_{\boldsymbol{R}} a_{\boldsymbol{R}} - V \sum_{\boldsymbol{R}} b^\dagger_{\boldsymbol{R}} b_{\boldsymbol{R}} \tag{3.13}$$

$$H_{pot} = V \sum_{\boldsymbol{k}} a^\dagger_{\boldsymbol{k}} a_{\boldsymbol{k}} - V \sum_{\boldsymbol{k}} b^\dagger_{\boldsymbol{k}} b_{\boldsymbol{k}} = \sum_{\boldsymbol{k}} \begin{pmatrix} a^\dagger_{\boldsymbol{k}} & b^\dagger_{\boldsymbol{k}} \end{pmatrix} \begin{pmatrix} V & 0 \\ 0 & -V \end{pmatrix} \begin{pmatrix} a_{\boldsymbol{k}} \\ b_{\boldsymbol{k}} \end{pmatrix} \tag{3.14}$$

We rewrite the hamiltonian in terms of the Pauli matrices:

$$\mathcal{H} = \mathcal{H}_{NN} + \mathcal{H}_{POT} = \mathcal{H}_0 \mathbb{1} + \mathcal{H}_x \sigma_x + \mathcal{H}_y \sigma_y + \mathcal{H}_z \sigma_z$$

$$\begin{aligned} \mathcal{H}_0 &= \frac{\mathcal{H}_{11} + \mathcal{H}_{22}}{2} = 0 \\ \mathcal{H}_z &= \frac{\mathcal{H}_{11} - \mathcal{H}_{22}}{2} = V \\ \mathcal{H}_x &= Re[\mathcal{H}_{21}] = -t\left[1 + cos(\boldsymbol{k}\cdot\boldsymbol{e}_1) + cos(\boldsymbol{k}\cdot\boldsymbol{e}_2)\right] \\ \mathcal{H}_y &= Im[\mathcal{H}_{21}] = t\left[sin(\boldsymbol{k}\cdot\boldsymbol{e}_1)) + sin(\boldsymbol{k}\cdot\boldsymbol{e}_2)\right] \end{aligned} \tag{3.15}$$

The only term different from the results of the previous section (eq.(3.7)) is $\mathcal{H}_z$, which is no longer 0. Using result (2.40), we know the dispersion relations for this model are:

$$\begin{aligned} \epsilon^{\pm} &= \pm\sqrt{t^2\left[3 + 2cos(\vec{k}\vec{e_1}) + 2cos(\vec{k}\vec{e_2}) + 2cos(\vec{k}(\vec{e_2} - \vec{e_1}))\right] + V^2} \\ &= \pm\sqrt{t^2\left[2 + 2cos(k_x) + 4cos(\frac{k_x}{2})cos(\frac{\sqrt{3}k_y}{2})\right] + V^2} \end{aligned} \tag{3.16}$$

At K and K' points, the energy is no longer degenerate. There is a gap between the two bands:

$$\Delta\epsilon(\boldsymbol{K}) = \Delta\epsilon(\boldsymbol{K'}) = 2|\mathcal{H}_z| = 2|V| \tag{3.17}$$

The system is now an insulator. Plots of the energy bands are shown in Figures 3.7a and 3.7b, just as in the previous section. It is clear that the bands don't cross nor touch.

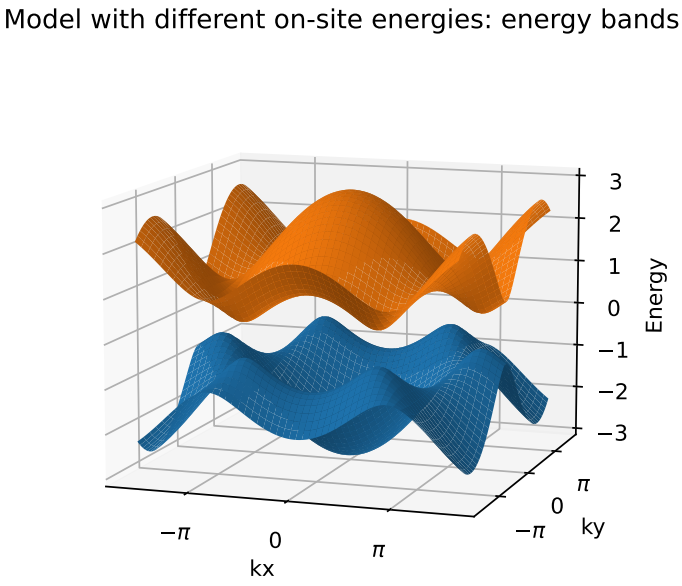

(a)

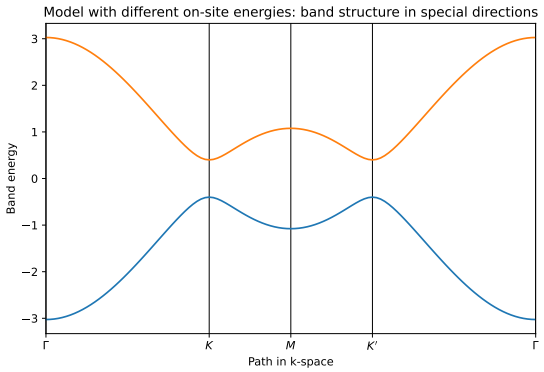

(b)

Figure 3.7: Energy bands for honeycomb lattice with real NN and complex and diferent on site energies for atoms on sites A and B. $t = 1.0$, $V = 0.4$.

Computing the topological index of the bands gives the following results:

$$\begin{aligned} \text{Upper band:} \quad & \text{Berry flux} = 0.0 \longrightarrow C = 0 \\ \text{Lower band:} \quad & \text{Berry flux} = 0.0 \longrightarrow C = 0 \end{aligned}$$

In conclusion, the system is a trivial insulator. This was expected, since time-reversal symmetry has been preserved.

We can arrive at the same conclusion by inspecting the eingenvectors of $\mathcal{H} = \mathcal{H}_{NN} + \mathcal{H}_{POT}$. Since $\mathcal{H}_z = V$ always has the same sign, the eigenvectors have no singularities and we can compute the integral of the Berry curvature $\mathcal{F}$ using the same expression over the whole Brillouin zone. Then, according to what was explained in section 2.3.6, we expect $C = 0$.

3.5 Introducing NNN complex hoppings

In order to have a topologically nontrivial insulator, we must break time-reversal symmetry. For that purpose, as proposed by Haldane, we add complex hoppings to the system. We return to the monatomic honeycomb lattice with NN real hoppings, and add next nearest neighbour (NNN) complex hoppings. There is no on-site energy difference, and inversion symmetry is not broken.

The complex hoppings can be attributed to the effect of a magnetic field on the electron, which adds a complex phase to the wave function by the Aharonov-Bohm effect. The complex phase picked up by the electron when moving in a magnetic field is proportional to a line integral of the magnetic potential trough the path.

This is not an external uniform field (like in the Quantum Hall Effect). With a staggered magnetic field the net flux through a unit cell can be zero, and the periodicity of the lattice is maintained [9].

If the magnitude of the hopping from A to B is $-t'e^{i\theta}$, the magnitude of hopping form B to A is the complex conjugate (so $-t'e^{-i\theta}$), because the phase gained by the wave function is of opposite sign. This is also necessary for the hamiltonian to be hermitian.

We want to choose the hoppings in a manner that maintains the characteristic 6-fold symmetry of the lattice (see Figure 3.8). Hoppings following the arrows are taken to have magnitude $-t'e^{i\theta}$, and for the hoppings going in the opposite direction we take $-t'e^{-i\theta}$.

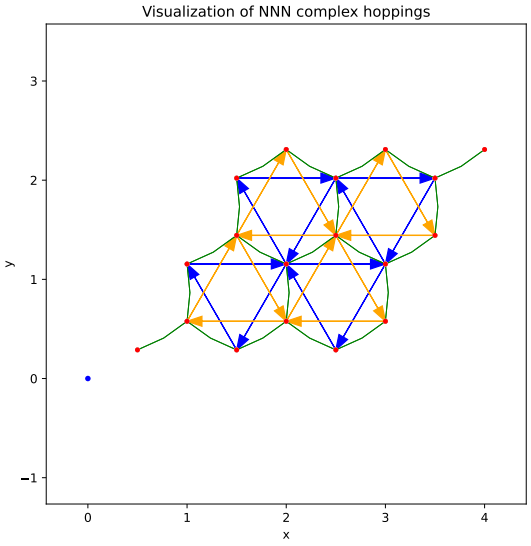

Figure 3.8: Visualization of A-A (blue) and B-B (orange) complex hoppings.

We now proceed to construct the hamiltonian corresponding to the system, following the same procedure as in previous sections. To the hamiltonian H_{NN} from equation 3.6 we need to add H_{NNN}, which contains the kinetic energy from the NNN hoppings. Since the complex hoppings connect atoms of the same type, H_{NNN} is only going to add diagonal elements to the kernel.

We have 6 NNN hoppings per unit cell, 3 of the type A-A and 3 of type B-B (plus another 6 going in the opposite direction). I will use these to construct H_{NNN}:

$$\begin{gathered} A(0,0) \to A(1,0),\ A(0,0) \xrightarrow{\dagger} A(0,1),\ A(0,0) \xrightarrow{\dagger} A(1,-1) \\ B(0,0) \xrightarrow{\dagger} B(1,0),\ B(0,0) \to B(0,1),\ B(0,0) \to B(1,-1) \end{gathered}$$

Hoppings going in the opposite direction form arrows in Figure 3.8 are indicated with "†". So, the hamiltonian is:

$$\begin{aligned} H_{NNN} = &-t'e^{i\theta}\sum_i a^\dagger_{\boldsymbol{R}} a_{\boldsymbol{R}+\boldsymbol{e}_1} - t'e^{-i\theta}\sum_i a^\dagger_{\boldsymbol{R}} a_{\boldsymbol{R}+\boldsymbol{e}_2} - t'e^{-i\theta}\sum_i a^\dagger_{\boldsymbol{R}} a_{\boldsymbol{R}+\boldsymbol{e}_1-\boldsymbol{e}_2} \\ &-t'e^{-i\theta}\sum_i b^\dagger_{\boldsymbol{R}} b_{\boldsymbol{R}+\boldsymbol{e}_1} - t'e^{i\theta}\sum_i b^\dagger_{\boldsymbol{R}} b_{\boldsymbol{R}+\boldsymbol{e}_2} - t'e^{i\theta}\sum_i b^\dagger_{\boldsymbol{R}} b_{\boldsymbol{R}+\boldsymbol{e}_1-\boldsymbol{e}_2} + h.c. \end{aligned} \tag{3.18}$$

We again transform our hamiltonian into k-space:

$$\begin{aligned} H_{NNN} = &-t'e^{i\theta}\sum_{\boldsymbol{k}} a^\dagger_{\boldsymbol{k}} a_{\boldsymbol{k}} e^{i\boldsymbol{k}\cdot\boldsymbol{e}_1} - t'e^{-i\theta}\sum_{\boldsymbol{k}} a^\dagger_{\boldsymbol{k}} a_{\boldsymbol{k}} e^{i\boldsymbol{k}\cdot\boldsymbol{e}_2} - t'e^{-i\theta}\sum_{\boldsymbol{k}} a^\dagger_{\boldsymbol{k}} a_{\boldsymbol{k}} e^{i\boldsymbol{k}\cdot(\boldsymbol{e}_1-\boldsymbol{e}_2)} \\ &-t'e^{-i\theta}\sum_{\boldsymbol{k}} b^\dagger_{\boldsymbol{k}} b_{\boldsymbol{k}} e^{i\boldsymbol{k}\cdot\boldsymbol{e}_1} - t'e^{i\theta}\sum_{\boldsymbol{k}} b^\dagger_{\boldsymbol{k}} b_{\boldsymbol{k}} e^{i\boldsymbol{k}\cdot\boldsymbol{e}_2} - t'e^{i\theta}\sum_{\boldsymbol{k}} b^\dagger_{\boldsymbol{k}} b_{\boldsymbol{k}} e^{i\boldsymbol{k}\cdot(\boldsymbol{e}_1-\boldsymbol{e}_2)} + h.c. \\ = &-t'\sum_{\boldsymbol{k}} a^\dagger_{\boldsymbol{k}} a_{\boldsymbol{k}} \left(e^{i(\theta+\boldsymbol{k}\cdot\boldsymbol{e}_1)} + e^{-i(\theta-\boldsymbol{k}\cdot\boldsymbol{e}_2)} + e^{-i(\theta-\boldsymbol{k}\cdot\boldsymbol{e}_1+\boldsymbol{k}\cdot\boldsymbol{e}_2)}\right) \\ &-t'\sum_{\boldsymbol{k}} b^\dagger_{\boldsymbol{k}} b_{\boldsymbol{k}} \left(e^{-i(\theta-\boldsymbol{k}\cdot\boldsymbol{e}_1)} + e^{i(\theta+\boldsymbol{k}\cdot\boldsymbol{e}_2)} + e^{i(\theta+\boldsymbol{k}\cdot\boldsymbol{e}_1-\boldsymbol{k}\cdot\boldsymbol{e}_2)}\right) \\ &-t'\sum_{\boldsymbol{k}} a^\dagger_{\boldsymbol{k}} a_{\boldsymbol{k}} \left(e^{-i(\theta+\boldsymbol{k}\cdot\boldsymbol{e}_1)} + e^{i(\theta-\boldsymbol{k}\cdot\boldsymbol{e}_2)} + e^{i(\theta-\boldsymbol{k}\cdot\boldsymbol{e}_1+\boldsymbol{k}\cdot\boldsymbol{e}_2)}\right) \\ &-t'\sum_{\boldsymbol{k}} b^\dagger_{\boldsymbol{k}} b_{\boldsymbol{k}} \left(e^{i(\theta-\boldsymbol{k}\cdot\boldsymbol{e}_1)} + e^{-i(\theta+\boldsymbol{k}\cdot\boldsymbol{e}_2)} + e^{-i(\theta+\boldsymbol{k}\cdot\boldsymbol{e}_1-\boldsymbol{k}\cdot\boldsymbol{e}_2)}\right) \\ = &\sum_{\boldsymbol{k}} \begin{pmatrix} a^\dagger_{\boldsymbol{k}} & b^\dagger_{\boldsymbol{k}} \end{pmatrix} \begin{pmatrix} \mathcal{H}_{11} & 0 \\ 0 & \mathcal{H}_{22} \end{pmatrix} \begin{pmatrix} a_{\boldsymbol{k}} \\ b_{\boldsymbol{k}} \end{pmatrix} \end{aligned} \tag{3.19}$$

where:

$$\begin{aligned}\mathcal{H}_{11} &= -2t'\left(cos(\theta + \boldsymbol{k}\cdot\boldsymbol{e_1}) + cos(\theta - \boldsymbol{k}\cdot\boldsymbol{e}_2) + cos(\theta - \boldsymbol{k}\cdot\boldsymbol{e}_1 + \boldsymbol{k}\cdot\boldsymbol{e}_2)\right)\\ \mathcal{H}_{22} &= -2t'\left(cos(\theta - \boldsymbol{k}\cdot\boldsymbol{e}_1) + cos(\theta + \boldsymbol{k}\cdot\boldsymbol{e}_2) + cos(\theta + \boldsymbol{k}\cdot\boldsymbol{e}_1 - \boldsymbol{k}\cdot\boldsymbol{e_2})\right)\end{aligned} \tag{3.20}$$

The non-diagonal elements are the ones from H_{NN} in equation (3.6), so $\mathcal{H}_x$ and $\mathcal{H}_y$ are the same as in equation (3.7). The kernel in terms of the Pauli matrices:

$$\begin{aligned}\mathcal{H}_0 &= \frac{\mathcal{H}_{11}+\mathcal{H}_{22}}{2} = -2t'cos(\theta)\left[cos(\boldsymbol{k}\cdot\boldsymbol{e_1}) + cos(\boldsymbol{k}\cdot\boldsymbol{e_2}) + cos(\boldsymbol{k}\cdot(\boldsymbol{e}_1-\boldsymbol{e}_2))\right]\\ \mathcal{H}_z &= \frac{\mathcal{H}_{11}-\mathcal{H}_{22}}{2} = 2t'sin(\theta)\left[sin(\boldsymbol{k}\cdot\boldsymbol{e_1}) - sin(\boldsymbol{k}\cdot\boldsymbol{e_2}) - sin(\boldsymbol{k}\cdot(\boldsymbol{e}_1-\boldsymbol{e}_2))\right]\\ \mathcal{H}_x &= Re[\mathcal{H}_{21}] = -t\left[1 + cos(\boldsymbol{k}\cdot\boldsymbol{e_1}) + cos(\boldsymbol{k}\cdot\boldsymbol{e_2})\right]\\ \mathcal{H}_y &= Im[\mathcal{H}_{21}] = t\left[sin(\boldsymbol{k}\cdot\boldsymbol{e_1}) + sin(\boldsymbol{k}\cdot\boldsymbol{e_2})\right]\end{aligned} \tag{3.21}$$

Or, in terms of k_x and k_y:

$$\begin{aligned}\mathcal{H}_0 &= -2t'cos(\theta)\left[cos(k_x) + 2cos(\frac{k_x}{2})cos(\frac{\sqrt{3}k_y}{2})\right]\\ \mathcal{H}_z &= 2t'sin(\theta)\left[sin(k_x) - 2sin(\frac{k_x}{2})sin(\frac{\sqrt{3}k_y}{2})\right]\\ \mathcal{H}_x &= -t\left[1 + cos(\frac{k_x}{2}) + cos(\frac{k_x}{2} + \frac{\sqrt{3}k_y}{2})\right]\\ \mathcal{H}_y &= t\left[sin(\frac{k_x}{2}) + sin(\frac{k_x}{2} + \frac{\sqrt{3}k_y}{2})\right]\end{aligned} \tag{3.22}$$

The dispersion relation $\epsilon^{\pm} = \mathcal{H}_0 \pm \sqrt{\mathcal{H}_x^2 + \mathcal{H}_y^2 + \mathcal{H}_z^2}$ has a messy expression for the general case, which I am not going to write explicitly. With the help of the program, we can compute the eigenvalues and see the energy bands graphically (Figure 3.9a and 3.9b).

It is clear that the degenerate points K, K' are no longer there. As expected, braking time-reversal symmetry opened a gap, and the system is now again an insulator. Let's compute the value of the energy gap at these points:

$$\begin{aligned}k = K = \left(-\frac{1}{3}, \frac{1}{3}\right) \longrightarrow \mathcal{H}_x &= -t\left[cos(\frac{-2\pi}{3}) + cos(\frac{2\pi}{3}) + cos(0)\right] = -t[-\frac{1}{2} - \frac{1}{2} + 1] = 0\\ \mathcal{H}_y &= t\left[sin(\frac{-2\pi}{3}) + sin(\frac{2\pi}{3})\right] = -t[-\frac{\sqrt{3}}{2} + \frac{\sqrt{3}}{2}] = 0\\ \mathcal{H}_z &= -2t'sin(\theta)\left[sin(\frac{-2\pi}{3}) - sin(\frac{2\pi}{3}) + sin\frac{4\pi}{3}\right] = -3\sqrt{3}t'sin\theta\end{aligned} \tag{3.23}$$

$$k = K' = \left(\frac{1}{3}, -\frac{1}{3}\right) \longrightarrow \mathcal{H}_x = \mathcal{H}_y = 0, \;\; \mathcal{H}_z = 3\sqrt{3}t' sin\theta \tag{3.24}$$

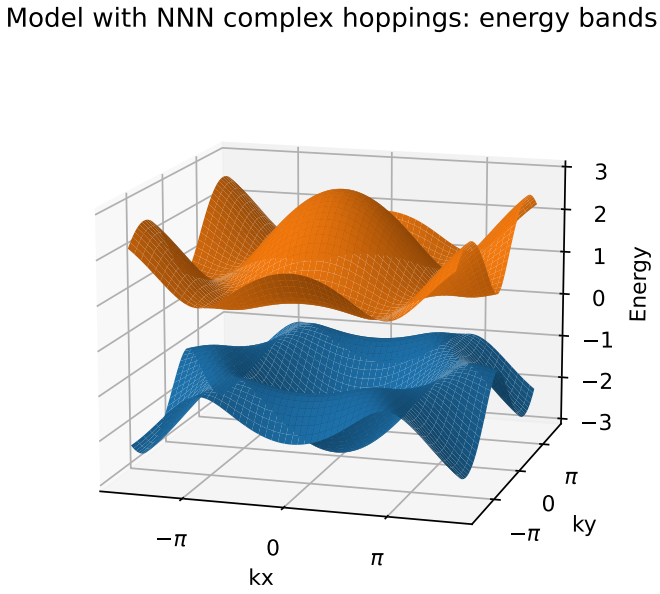

(a)

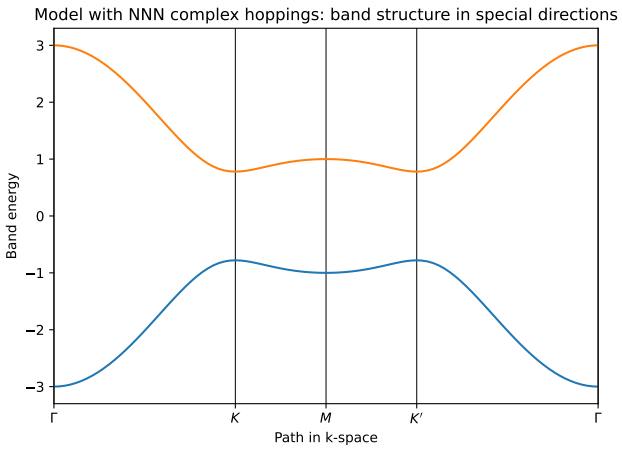

(b)

Figure 3.9: Energy bands for honeycomb lattice with real NN and complex NNN hoppings. $t = 1.0$, $t' = 0.15$, $\theta = \frac{\pi}{2}$.

In both cases:

$$\Delta\epsilon = 2\sqrt{\mathcal{H}_x^2 + \mathcal{H}_y^2 + \mathcal{H}_z^2} = 2|\mathcal{H}_z| = 6\sqrt{3}t' sin\theta \tag{3.25}$$

Which is not 0 unless $\theta = n\pi$. In that case, the term for the NNN hoppings would be purely real: $-t'e^{i\theta} = -t'$ or $-t'e^{i\theta} = +t'$. Time-reversal symmetry would not be broken, so the system would conserve both time-reversal and inversion symmetry, and in consequence, the Dirac points.

Let's now examine the eigenvectors. $\mathcal{H}_z$ is positive at K point but negative at K', for any choice of gauge, so we have to use two different expressions for the Bloch waves over the Brillouin zone to calculate the Berry flux. This singularity points out the fact that the system is a topological insulator.

As expected, when computing the Berry flux and Chern number for each of the bands, we get:

$$\begin{aligned} &\text{Upper band:} && \text{Berry flux} = 6.283185 \longrightarrow C = 1 \\ &\text{Lower band:} && \text{Berry flux} = -6.283185 \longrightarrow C = -1 \end{aligned}$$

In conclusion, we have constructed a topologically insulating system by braking time-reversal symmetry. Even if figures 3.7 and 3.9 look similar, one might say they are geometrically equivalent, they are different from the topological point of view.

3.6 Haldane's model with different topological phases

The last step is to consider a system with NN real hoppings, different on-site energies and NNN complex hoppings. This system hast lost both inversion and time reversal symmetries.

Putting it all together, the complete hamiltonian is going to be:

$$H = H_{NN} + H_{NNN} + H_{POT} \tag{3.26}$$

The kernel in terms of the Pauli matrices:

$$\begin{aligned} \mathcal{H}_0 &= \frac{\mathcal{H}_{11} + \mathcal{H}_{22}}{2} = -2t' cos(\theta)\left[cos(\boldsymbol{k}\cdot\boldsymbol{e}_1) + cos(\boldsymbol{k}\cdot\boldsymbol{e}_2) + cos(\boldsymbol{k}\cdot(\boldsymbol{e}_1 - \boldsymbol{e}_2))\right] \\ \mathcal{H}_z &= \frac{\mathcal{H}_{11} - \mathcal{H}_{22}}{2} = 2t' sin(\theta)\left[sin(\boldsymbol{k}\boldsymbol{e}_1) - sin(\boldsymbol{k}\cdot\boldsymbol{e}_2) + sin(\boldsymbol{k}\cdot(\boldsymbol{e}_1 - \boldsymbol{e}_2))\right] + V \\ \mathcal{H}_x &= Re[\mathcal{H}_{21}] = -t\left[1 + cos(\boldsymbol{k}\cdot\boldsymbol{e}_1) + cos(\boldsymbol{k}\cdot\boldsymbol{e}_2)\right] \\ \mathcal{H}_y &= Im[\mathcal{H}_{21}] = t\left[sin(\boldsymbol{k}\cdot\boldsymbol{e}_1) + sin(\boldsymbol{k}\cdot\boldsymbol{e}_2)\right] \end{aligned} \tag{3.27}$$

The only difference with equation (3.21) is that we must add V to $\mathcal{H}_z$. So at the K and K' points, the energy gaps are now:

$$k = K = \left(-\frac{1}{3}, \frac{1}{3}\right) \longrightarrow \mathcal{H}_x = \mathcal{H}_y = 0,\ \ \mathcal{H}_z = -3\sqrt{3}t' sin\theta + V$$
$$\Delta\epsilon(\vec{K}) = 2|V - 3\sqrt{3}t' sin\theta| \tag{3.28}$$

$$k = K' = \left(\frac{1}{3}, -\frac{1}{3}\right) \longrightarrow \mathcal{H}_x = \mathcal{H}_y = 0,\ \ \mathcal{H}_z = 3\sqrt{3}t' sin\theta + V$$
$$\Delta\epsilon(\vec{K'}) = 2|V + 3\sqrt{3}t' sin\theta| \tag{3.29}$$

The sign of $\mathcal{H}_z$ depends on the relation between parameters t', θ and V. We have constructed a system that, when changing the values of such parameters, is in different topological phases.

- $\boldsymbol{|V| > |3\sqrt{3}t' sin\theta|}$ **: Topologically trivial insulator**

In this case, $\mathcal{H}_z$ will have the same sign at K and K'. There are no singularities in the eigenvectors, and it is possible to calculate the Berry flux with the same Bloch vector for the whole Brillouin zone. The situation is the same as for when we had the NN hoppings and different on-site energies only (section 3.4): the system is a trivial insulator.

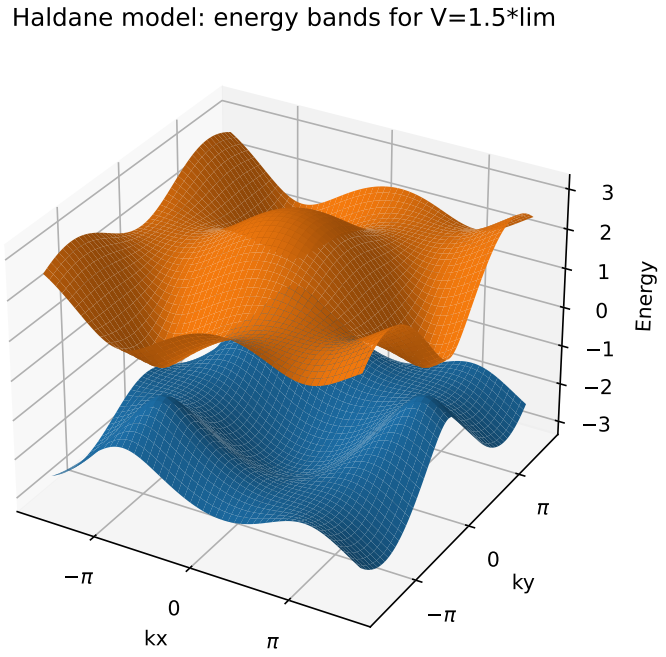

Figure 3.10: Surface plot of electronic energy bands for Haldane's model in trivial phase. $t = 1.0$, $t' = 0.15$, $\theta = \frac{\pi}{2}$, $V = 1.5 \cdot \text{lim}$.

Figure 3.10 shows a surface plot of the energy bands for this regime. I have defined lim=$3\sqrt{3}t'sin\theta$ for simplicity. Computational calculations of the Berry flux and Chern number for these values confirm the system is a trivial insulator:

$$\begin{aligned} \text{Upper band:} \quad & \text{Berry flux} = 0.0 \longrightarrow C = 0 \\ \text{Lower band:} \quad & \text{Berry flux} = 0.0 \longrightarrow C = 0 \end{aligned}$$

- $\boldsymbol{|V| < |3\sqrt{3}t'sin\theta|}$ **: Topological insulator**

For these values of V, $\mathcal{H}_z$ has opposite sign at $\boldsymbol{k} = \boldsymbol{K}$ and $\boldsymbol{k} = \boldsymbol{K}$, just as it was for the case of real NN hoppings plus complex NNN hoppings in section 3.5. There is a singularity in the eigenvectors and this tells us that the topological index is nonzero: the system is a topological insulator.

Figure 3.11 shows a surface plot of the energy bands. Results of Berry flux calculations for this regime, are:

$$\begin{aligned} \text{Upper band:} \quad & \text{Berry flux} = 6.283185 \longrightarrow C = 1 \\ \text{Lower band:} \quad & \text{Berry flux} = -6.283185 \longrightarrow C = -1 \end{aligned}$$

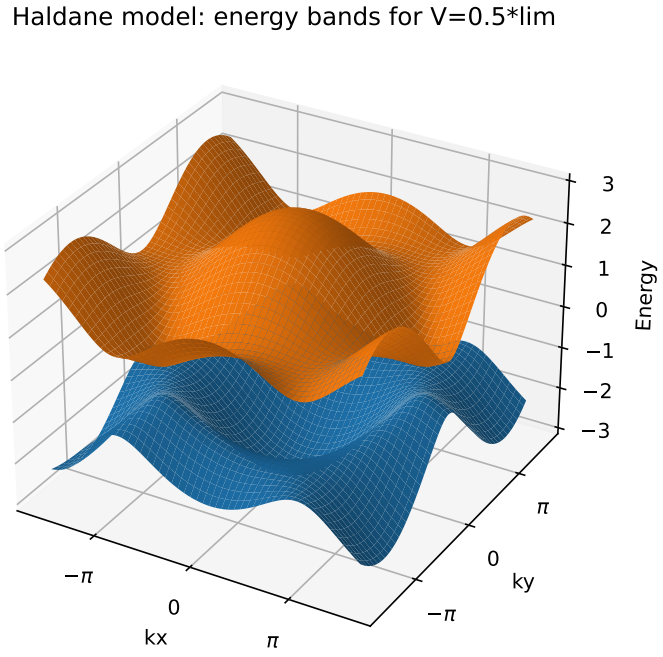

Figure 3.11: Surface plot of electronic energy bands for Haldane's model in topological phase.

- $\boldsymbol{|V| = |3\sqrt{3}t'sin\theta|}$ **: Topological transition**

When $|V| = |3\sqrt{3}t'sin\theta|$, the gap closes at one point: at $\boldsymbol{k} = \boldsymbol{K}$ if V and $3\sqrt{3}t'sin\theta$ are of the same sign, or at $\boldsymbol{k} = \boldsymbol{K'}$ if they are of opposite sign. In this situation, the two bands just touch, and for the case of graphene, the system is a semi-metal as in section 3.3. Figure 3.12 shows a surface plot of the energy bands.

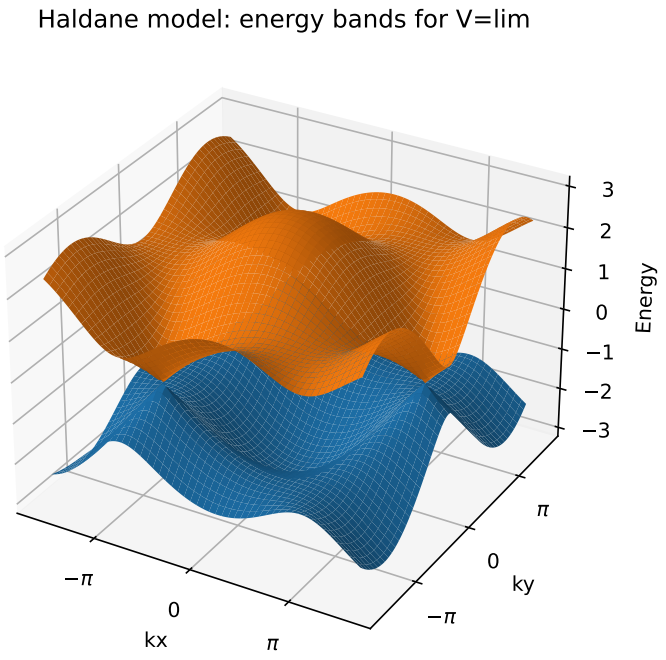

Figure 3.12: Surface plot of electronic energy bands for Haldane's model at topological transition point.

This state in a topological transition, and connects the two distinct topological phases. We have confirmed that, in order to have a topological transition, the gap must be closed and reopened (as explained in section 2.3.3).

Figure 3.13 shows a sequence of graphs that show the band structure of Haldane's model for different values of V. One can clearly see the two different topological domains and the topological transition between them. Figure 3.14 shows the density of states as a function of energy, for the same systems as in figure 3.13. At the topological transition state V=lim, 0 energy eingenstates appear.

Note that I have taken negative values for V, which, from its definition in section 3.4 implies that atoms on site A have lower energy than those on site B. If it was the other way around, V would be positive (opposite sign from t') and the remaining Dirac point would be K' instead of K.

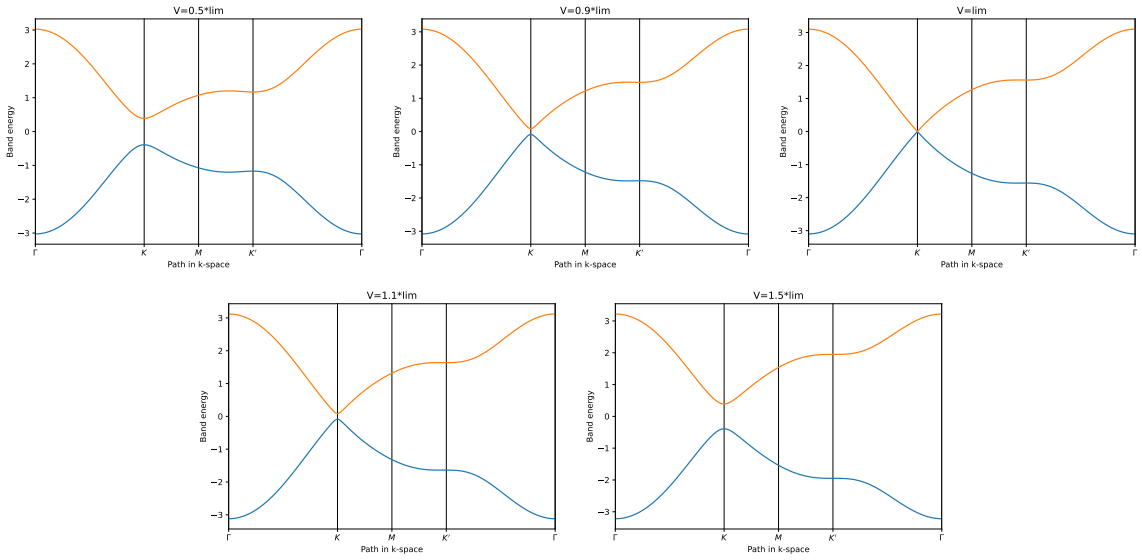

Figure 3.13: 2D projection of the band structure along a path in k-space of Haldane's model with different values of V.

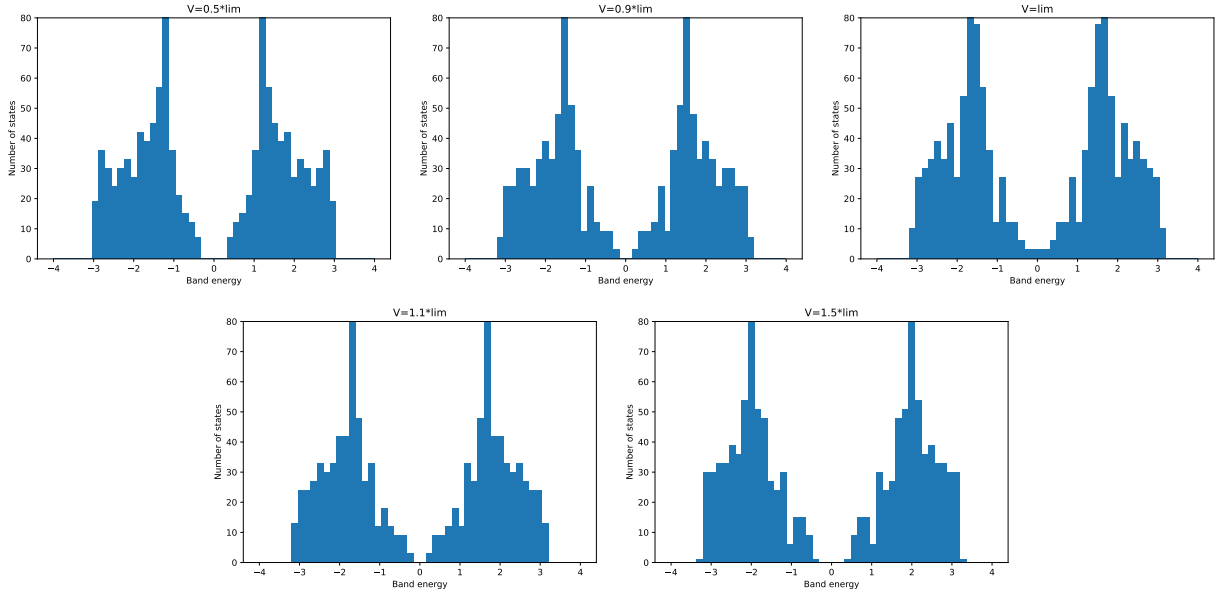

Figure 3.14: Density of states as a function of energy for Haldane's model with different values of V

3.7 Finite systems and edge states

In the previous section, in our study of Haldane's model, we have considered systems with periodic boundary conditions in both spacial directions. This resulted in a Brillouin zone periodic in both directions of k-space, that could be regarded as a closed manifold.

The most interesting phenomena occurs in finite systems, where we have topologically protected edge states. In finite systems only one (or none) direction is regarded as infinite, so we only have periodic boundary conditions (PBC) in that direction.

Let's study Haldane's model in a honeycomb lattice with PBC in direction $\boldsymbol{e}_1$ but finite in direction $\boldsymbol{e}_2$. The unit cell is going to be a "strip" in the $\boldsymbol{e}_2$ direction (see Figure 3.15). This unit cell is equivalent to N of to the previous unit cells (Figure 3.2), stacked in the $\boldsymbol{e}_2$ direction.

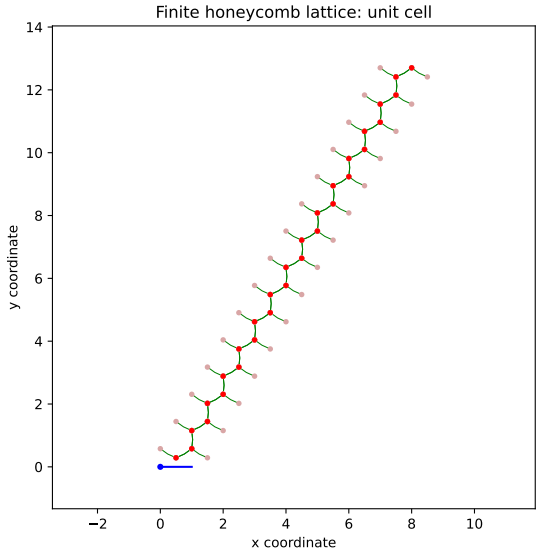

Figure 3.15: Unit cell for a honeycomb lattice with PBC in the $\vec{e_1}$ direction and NN hoppings. N=15.

There are $2N$ sites in this unit cell, so there will be $2N$ energy states for each vector $\boldsymbol{k}$, that together form $2N$ one-dimensional energy bands.

A section of this lattice would look the same as Figure 3.1. Notice that the A and B sites at the edges of the system (top and bottom) form a *zig-zag* shape. There is also another possible configuration: imagine tilting the lattice slightly so that the A and B sites lie in the same horizontal line (this configuration is often called *armchair*). The shape of the edges affects the geometry of the band structure, so it is important to mention which configuration was chosen.

There is no translational symmetry along y (due to the existence of the edge), so we cannot define common eigenstates for H, k_x and k_y, but we can still find eigenstates for H

and k_x, because they commute with each other:

$$|\Psi_{n,k_x}> \qquad\qquad \epsilon_{n,k_x}$$

where n =1,2,...,2N. Since we only have one symmetry direction the reciprocal lattice is one dimensional, a chain of sites with spacing 2π.

I have calculated the energy eigenstates computationally, and the resullts are shown in Figure 3.16.

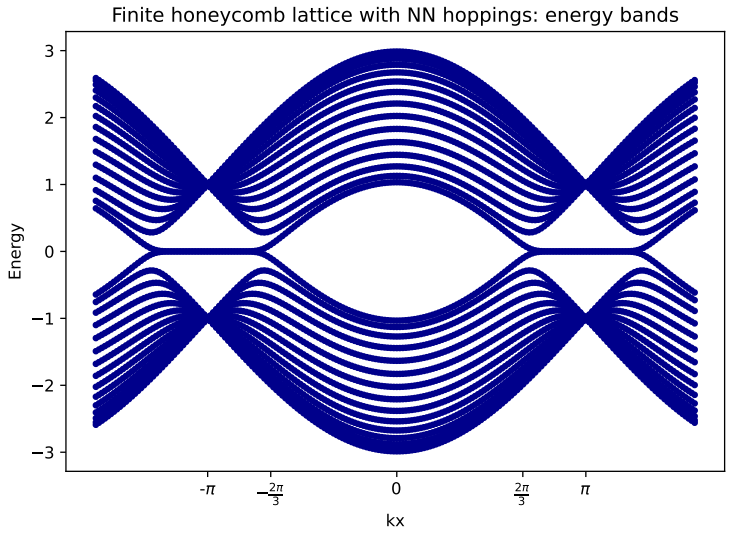

Figure 3.16: Electronic energy band structure for a honeycomb lattice with PBC in the $\vec{e_1}$ direction and NN hoppings. n=15.

In Figure 3.16 we see the 2D projection of the 3D upper and lower energy bands. The two Dirac cones can be identified at the edges of the Brillouin zone at $k_x = -\frac{2\pi}{3}$ and $k_x = \frac{2\pi}{3}$. As expected, the system is gapless, and it is degenerate at $\epsilon = 0$.

When perturbing the system, the vertices of the degenerate energy states (at the projection of the Dirac points) will remain attached to the upper or lower band. So there are two possibilities: both edges are connected to the same band and we have a trivial insulator with a gap, or they connect to different bands and the conducting edge states will connect the valence and conduction bands. The former is the case for a topological insulator.

Now let's consider the finite version of Haldane's model, and see the results on the different topological regimes. Figure 3.17 shows the existence of the conducting edge states in the topological regime, the phase transition (where not only the edge states, but the energy bands corresponding to the bulk, touch), and the trivial regime with a clear energy gap.

We stated that the degenerate bands correspond to the edge states. To arrive at that conclusion we must inspect the eigenvectors. Since the components of the eigenvectors are the coefficients of the Bloch-like expansion in the position baisis (equation (2.28)), they give us information of the weight of each localized orbital in the wave function.

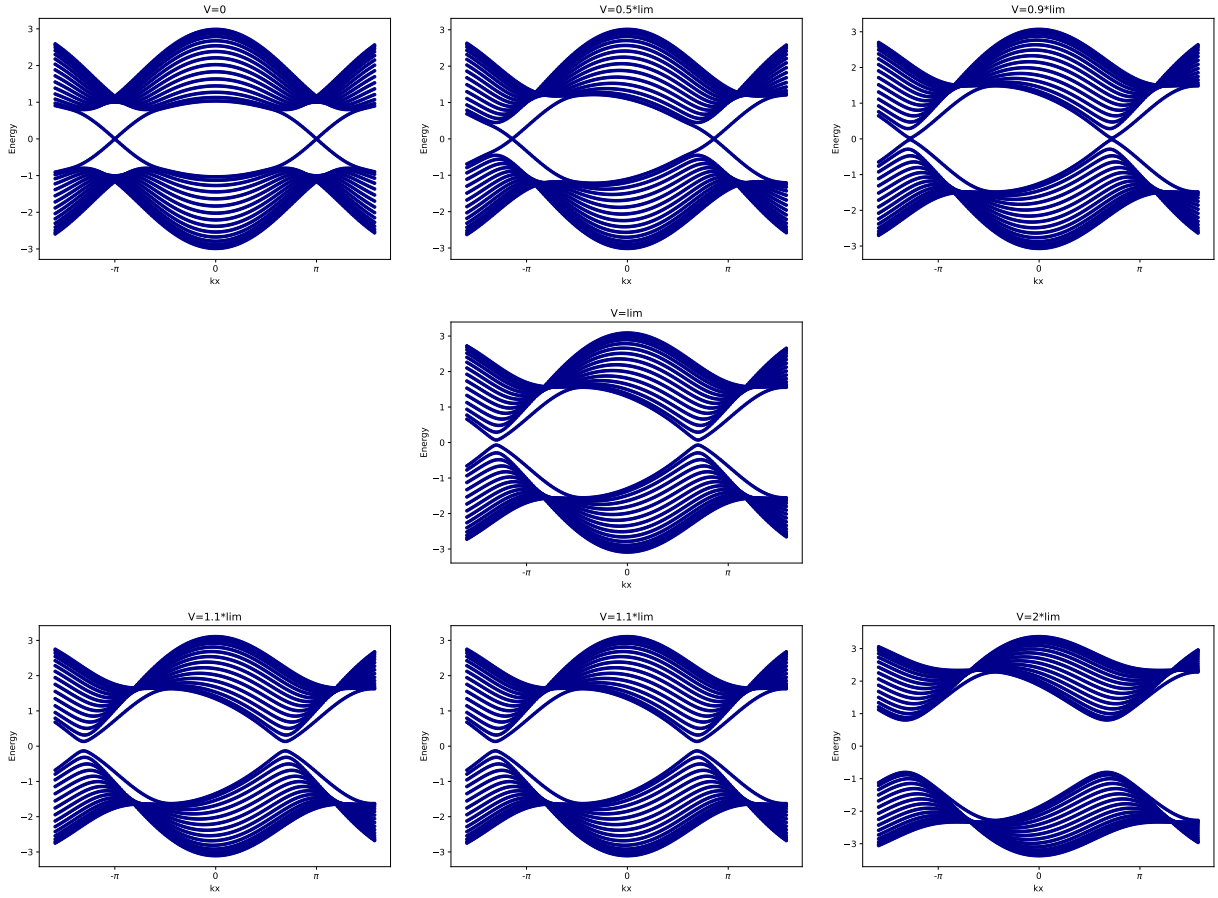

Figure 3.17: Band structure for a finite Haldane model in the different topological regimes.

Let us take the case for V=0 (first image of Figure 3.17) and solve for the eigenvetors for $k_x = \pi$. The eigenvectors corresponding to the degenerate eigenvalue $\epsilon = 0$ are calculated to be:

$$u_{29} = -0.23374 - 0.12728i, \quad u_{30} = 0.96057 - 0.02310i \longrightarrow |u_{29}|^2 + |u_{30}|^2 = 0.99411 \quad (3.30)$$

$$u_1 = 0.96087, \quad u_2 = 0.23049 + 0.13307i \longrightarrow |u_1|^2 + |u_2|^2 = 0.99411 \quad (3.31)$$

In both eigenvectors all other 28 coefficients are more than a magnitude smaller than the ones given. We conclude that for the first case, the state is localized at the lower edge of the lattice. For the second case, the state is localized at the top edge.

Chapter 4
Conclusion

In summary, Haldane came up with a sensible way of braking time reversal symmetry in the honeycomb lattice, and realized this resulted in the anomalous quantum hall effect, that appears as an intrinsic property of the band structure. The topological phase of this type of topological insulator can be characterized by the Chern number C, and that the different topological regimes are connected by a band closing point. The emergence of edge states has been demonstrated when studying the finite system, and a direct consequence of the topological invariance is the robustness of these quantum states.

This study of Haldane's model has shown that tight binding models can be used to arrive at useful results, regardless of their simplicity. Combined with the second quantization formalism, we have built a formal way to arrive at the dispersion relations and Bloch waves for any tight-binding system.

Even if the analytical study of simple tight binding models is possible, computational calculations greatly ease the task, specially in more complex models. The PythTB package has demonstrated to be adequate for that purpose, as well as for Berry flux calculations.

We have seen that a NN hopping model for graphene results in symmetrically protected Dirac points and Dirac cones. This system has the property of not having an energy gap, but also no partially filled band. A slight tuning can make the Fermi energy rise or lower, resulting in a partially filled band. This behaviour is reminiscent of that of a semiconductor, and using graphene in the same way as a semiconductor is one of its possible applications.

The topic covered in this work is only a very small fraction of the theory of topological insulators. There are many more types of topological insulators in two and three dimensions, that are characterized by different topological invariants. The natural next step would be to study the model for graphene proposed by C.L. Kane and E.J. Mele in 2005 [14] (also known as the Quantum Hall Spin effect). This system acquires the topological phase by means of spin orbit coupling, while time-reversal symmetry is maintained.

As a final comment, the experimental realization of two and three-dimensional topological insulators has been achieved in recent years [15] [16], and both the theoretical and experimental fields of topological matter are very active nowadays.

Bibliography

[1] Sinisa Coh and David Vanderbilt. *PythTB 1.7.2 documentation*. URL: https://www.physics.rutgers.edu/pythtb/about.html.

[2] David N Mermin Neil W. Ashcroft. "Solid State Physics". In: Harcourt College Publishers, 1976. Chap. 8.

[3] Kai Sun. *Second quantization and tight binding models*. URL: http://www-personal.umich.edu/~sunkai/teaching/Fall_2012/phys620.html.

[4] Franz Utermohlen. *Tight-Binding Model in the Second Quantization Formalism*. URL: https://www.physics.rutgers.edu/pythtb/about.html.

[5] Kai Sun. *Tight binding models part II*. URL: http://www-personal.umich.edu/~sunkai/teaching/Fall_2012/phys620.html.

[6] Kai Sun. *Berry connection, Berry curvature and Hall conductivity*. URL: http://www-personal.umich.edu/~sunkai/teaching/Fall_2012/phys620.html.

[7] Kai Sun. *Topological index, the Chern number and quantized Hall conductivity*. URL: http://www-personal.umich.edu/~sunkai/teaching/Fall_2012/phys620.html.

[8] Daniel Osadchy Joseph E. Avron and Ruedi Selier. "A Topological Look at the Quantum Hall Effect". In: *Physics today* 56 (2003), pp. 38–42.

[9] Kai Sun. *Tight binding models part III*. 2012. URL: http://www-personal.umich.edu/~sunkai/teaching/Fall_2012/phys620.html.

[10] F. D. M. Haldane. "Model for a Quantum Hall Effect without Landau Levels: Condensed-Matter Realization of the "Parity Anomaly"". In: *Phys. Rev. Lett.* 61 (18 1988), pp. 2015–2018.

[11] Sinisa Coh and David Vanderbilt. *PythTB 1.7.2 documentation*. URL: https://www.physics.rutgers.edu/pythtb/about.html.

[12] Ganhua Lu et al. "Semiconducting graphene: converting graphene from semimetal to semiconductor". In: *Nanoscale* 5 (4 2013), pp. 1353–1368.

[13] K. S. Novoselov et al. "Two-dimensional atomic crystals". In: *Proceedings of the National Academy of Sciences* 102.30 (2005), pp. 10451–10453.

[14] C. L. Kane and E. J. Mele. "Quantum Spin Hall Effect in Graphene". In: *Phys. Rev. Lett.* 95 (22 2005), p. 226801.

[15] Cui-Zu Chang et al. "Experimental Observation of the Quantum Anomalous Hall Effect in a Magnetic Topological Insulator". In: *Science* 340.6129 (2013), pp. 167–170.

[16] Y. L. Chen et al. "Experimental Realization of a Three-Dimensional Topological Insulator, Bi2Te3". In: *Science* 325.5937 (2009), pp. 178–181.